Chapter 9

Thermal roughening of surfaces : experimental aspects

Klaus Kern

Institut de Physique Expérimentale, EPF-Lausanne, CH-1015 Lausanne, Switzerland

1 INTRODUCTION : THERMAL RESTRUCTURING AT SURFACES

The atoms in the surface of a crystal are missing part of their nearest neighbors which gives rise to a charge redistribution in the selvedge. This changed force field is responsible for noticeable interlayer relaxations in the near surface region. Intuitively the inward relaxation of the outermost surface layer can be explained by the tendency of the valence electrons to spill over the surface in order to create a lateral smoothing of the electronic charge density [1]. The new electron distribution causes electrostatic forces on the ion cores of the surface atoms, resulting in a contraction of the first interlayer spacing ($d_{12} < d_b$). This relaxation is most pronounced for open, loosely packed, surfaces. In addition, the changes in the force field can also favor lateral atomic rearrangements in the surface plane . The surface "reconstructs" into a phase with new symmetry. These reconstructive surface phase transitions can either occur spontaneously or be activated by temperature or by small amounts of adsorbates [2].

So far we have neglected the temperature of the system. As the temperature rises, however, the lattice vibrational amplitude increases and the anharmonic terms in the interaction potential gain importance. Due to the reduced number of nearest neighbors in the surface (a maximum of 9 at the surface of a fcc-crystal with respect to the 12 nearest neighbors in the bulk of this crystal) the mean-square amplitude of the surface atoms is much larger than in the bulk. While in bulk Cu, for example, anharmonicity is negligible below 70-80 % of the melting temperature, anharmonicity on the Cu(110) surface becomes important at temperatures above 40% of the melting temperature (the bulk Debye temperature of copper is $\theta_B = 343$ K, and the melting temperature is $T_M = 1356$ K).

At the high temperature end it has been demonstrated recently that on a variety of surfaces a disordered quasi-liquid layer wets the surface well below the bulk melting temperature, i.e. the melting of a crystal starts from the surface layer [3]. In view of the Lindemann criterion of melting [4], which states that melting occurs when the mean-square displacement of the atoms surpasses a critical value (~ 10% of the interatomic equilibrium distance), the important role that surfaces play in the melting phase transition is not surprising. As already discussed the mean vibrational amplitude is substantially enhanced at the surface and the Lindemann-criterion predicts a surface instability around 0.75 T_M.

The picture developed above is based on a perfect defect free surface, which is, however, only at zero temperature the stable equilibrium state. At elevated temperatures a certain amount of defects like isolated adatoms and vacancies as well as clusters of those can be thermally excited. Both adatom islands as well as vacancy holes are bordered by steps. Frenkel [5] studied the structure of such steps and argued that they should contain a large number of kinks at finite temperatures. Thus, due to thermal fluctuations, every crystal surface with steps should have a certain microscopic roughness

at nonzero temperature; the surface remains flat on macroscopic length scales however. Burton and coworkers, demonstrated that the thermal excitation of adatom and vacancy islands and thus the excitation of steps is negligible at low and medium temperatures but gave evidence for the presence of a roughening transition, at a temperature close to the bulk melting temperature, where the surface becomes macroscopically rough [6,7]. The critical temperature of this transition has been termed the roughening temperature, T_R. Burton et al. suggested that at the roughening temperature the free energy associated with the creation of a step vanishes. This was confirmed later by Swendsen in a detailed calculation [8]. One of the fundamental consequences of the existence of a roughening temperature for a certain crystallographic face below the melting temperature is that this face can occur on an equilibrium crystal only at temperatures below T_R.

Let us consider a surface which at $T = 0$ K is perfectly flat. Upon increasing the temperature, thermal fluctuations give rise to vacancies, adatoms and steps in the surface layer. The number of these "defects" increases until, at the roughening temperature, the long-range order of the surface disappears. Long-range order is confined here to the "height-correlation function" and not to the positional correlation function (parallel to the surface plane). Indeed, even above the roughening temperature, the surface atoms populate in average regular lattice sites. It is the fluctuation of the height $h(r)$ which diverges for temperatures $T > T_R$ [9].

$$g_\perp(r) \triangleq \langle [\, h(r') - h(0) \,]^2 \rangle \propto C(T)\ \ln(r) \qquad (1)$$

where C is a temperature-dependent constant and r a two-dimensional vector in a plane parallel to the surface. This divergence is very weak. At the roughening temperature $C(T_R) = 2/\pi^2$; the height fluctuation is one lattice spacing for a distance of 139 lattice spacings.

The first direct experimental evidence for a roughening transition was reported in 1979. Several groups had studied the thermal behavior of the basal plane of a hexagonal close-packed ^{4}He crystal [10]. In a beautiful experiment Balibar and Casting obtained for this surface a roughening temperature of $T_R \approx 1.2$ K.

More recently, the question of thermal roughening has also been addressed in the study of metal surfaces. Detailed He diffraction studies from the high Miller index (11n) surfaces of Cu [11] and Ni [12], with $n = 3, 5, 7$, proved the existence of a roughening transition on these surfaces.

The microscopic mechanism which leads to the roughening of a low and a high Miller index surface is, however, expected to be different. Indeed, as already mentioned, a low indexed surface – which at $T = 0$ K is perfectly flat – fulfills the roughening condition, Eq. (1), when the free energy for the creation of a step becomes zero. In contrast, on a high indexed surface – which at $T = 0$ K is already stepped – Eq. (1) can be fulfilled also without the creation of new steps. It appears that the proliferation of kinks is sufficient to

roughen the vicinal surface. Indeed, the ensuing meandering of the step rows, in conjunction with the mutual repulsion between these rows, leads also to the divergence of the "height-correlation function". Thus, the roughening temperature of high indexed surfaces is substantially lower than that of the low indexed ones. In the case of Cu and Ni (11n) the values for T_R range from 300 K to 720 K (Cu) and 450 K to 750 K (Ni) for n = 3, 5, 7.

While the existence of a roughening transition on stepped vicinal surfaces is undisputed, the basic question whether T_R of low indexed surfaces is lower than the crystal melting temperature T_M or not is still matter of discussion. The magnitude of T_R is governed by the bond strength at the surface. Thus, close packed surfaces with more neighbors and stronger bonds have a higher roughening temperature than more open surfaces. Indeed, while numerous fcc (110) surfaces have been found to undergo a roughening transition around 75% of the bulk melting temperature T_M, fcc (111) surfaces are generally believed to be stable up to T_M.

2 EQUILIBRIUM CRYSTAL SHAPE (ECS) AND SURFACE ROUGHENING

2.1 The surface free energy and the ECS

An interesting observation that puzzled scientists for several decades is the faceted equilibrium shape of single crystals. Intuitively it is clear that the ECS must somehow be related to the symmetry and energetics of the underlying atomic lattice. It was G. Wulff [13] who first made the connection between the microscopic and the macroscopie level. He demonstrated that the anisotropy of the surface free energy γ determines the ECS because a crystal will seek the shape that minimizes the total free energy of the surface at a given fixed crystal volume $\oint \gamma(\vartheta)\, dA$, here ϑ is a measure of the surface orientation and A the surface area. This amounts to a problem in affine geometry, the solution of which was given by Wulff : consider a polar plot of the surface free energy $\gamma(\vartheta)$, as illustrated in fig. 1 for a two-dimensional example. Draw a radius vector that intersects the polar plot at one point and makes a fixed angle with the horizontal and construct the plane that is perpendicular to the vector at the point of intersection. Then the inner envelope of all possible planes is the ECS [14].

The appearance of facets in the ECS is connected with the existence of cusps in the γ-plot. To see this we write down the surface free energy of a surface which is slightly misaligned with respect to a low-index Miller surface (fig. 2). Such a vicinal surface consists of flat close packed terraces of width n·a, separated by monatomic steps of height h. For large n the misalignement angle is $\vartheta \approx 1/n$. The surface free energy can be written in the form :

$$\gamma(\vartheta) = \gamma(0) + (\beta/h)\,|\vartheta| \qquad (2)$$

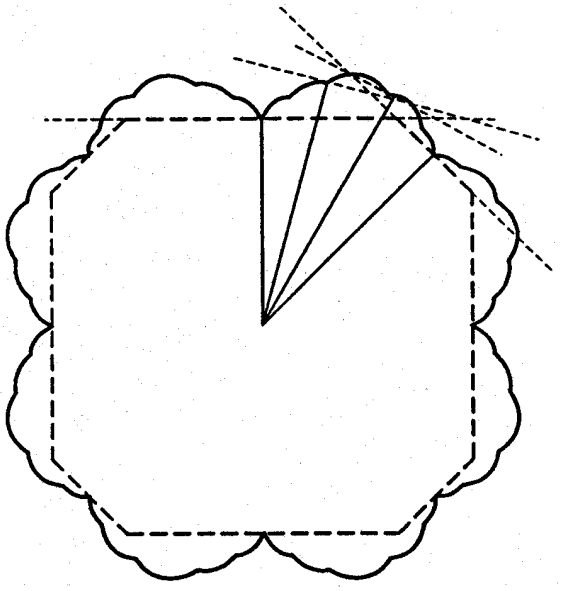

Figure 1. Polar plot of the total free surface energy γ (solid curve) and the Wulff construction of the equilibrium crystal shape (dashed curve) [14].

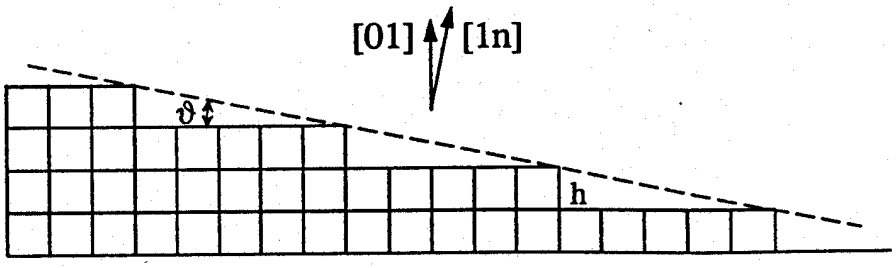

Figure 2. Schematic representation of a regularly stepped (vicinal) surface.

The first term $\gamma(\vartheta)$ is the free energy of the flat terrace while the second term adds the contribution from each of the monatomic steps, with β being the step free energy, i.e. the energy needed to produce a step on an otherwise flat surface. $\gamma(\vartheta)$ is a continuous function but has a non-analyticity, i.e. a cusp, at $\vartheta = 0$:

$$\Delta \left(\frac{d\gamma}{d\vartheta} \right)_{\vartheta = 0} = 2\beta/h \qquad (3)$$

The γ-plot (fig. 1) is thus characterized by cusps at orientations corresponding to low-index faces, which will show up as facets in the ECS. From the large number of cusps in the γ-plot at T = 0 K, however, only a small fraction, corresponding to the lowest Miller indices, will finally result in the appearence of facets in the ECS; i.e. the equilibrium crystal will be a sharp

polyhedron with few facets. FCC-crystals for instance are dominated by the two most densely packed surfaces (111) and (100).

In fig. 3 we illustrate this behavior for small lead crystals [15].

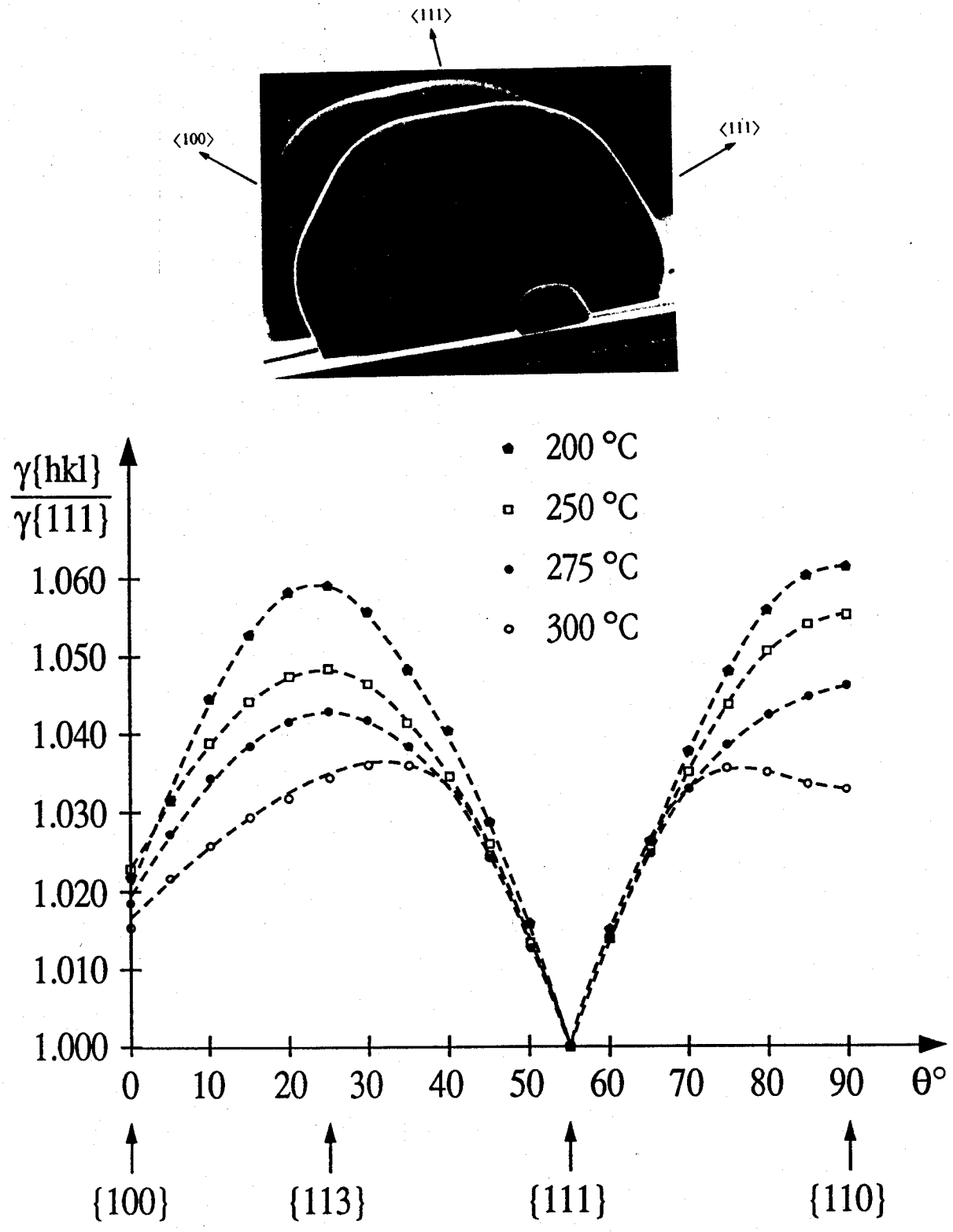

Figure 3. Electron microscopy image (a) of a lead crystal at 473 [15] and the anisotropy of γ (b) measured as a function of temperature [15].

2.2 The step free energy and the roughening transition in the ECS

In the discussion of the previous chapter we have ignored the temperature of the system (i.e. we have set $T = 0$ K). At 0 K the γ-plot is characterized by sharp cusps and the crystal is polyhedral, i.e. it is bounded entirely by facets. The facets in the ECS are microscopically flat with a minimum of surface defects. At nonzero temperature, however, surface defects can be excited thermally. The cusps in the γ-plot become blunt and in the ECS rounded regions appear, separating the facets at arbitrarily low nonzero temperature. As the temperature is further increased, the facets shrink and rounded regions grow. The blunting of the cusps and the corresponding strinking of the ECS-facets (i.e. the growing of the rounded step rich regions) is determined by the decrease of the step free energy, which is due at least partially to the entropic effects of kinks and kink wandering, since $f_{step}(T) = \beta(T) - T\, S_{step}(T)$. The free energy of steps vanishes at the roughening temperature with asymptotic dependence near T_R [8] :

$$\beta \propto \exp\left(-c/\sqrt{T_R - T}\right) \qquad (4)$$

At the roughening temperature, the step free energy becomes zero and the facet disappears. Above T_R the crystal surface is everywhere smoothly rounded. Smoothly rounded describes here the **macroscopic** morphology, which correspond on a microscopic scale to a very rough state with a high density of atomic steps. The step free energy depends of course upon the facet orientation. Thus, to every different stable facet corresponds a different roughening temperature. Heating an equilibrium crystal up, the different facets of the ECS disappear sequentially according to their respective T_R [16].

The roughening transition of a crystal surface can thus be detected by direct "visual" observation of the ECS. This approach is demonstrated below for the best studied example of the thermal evolution of the ECS : solid ^{4}He (hcp–crystallized) in coexistence with its own superfluid. Fig. 4 shows optical microscopy images of ^{4}He crystals taken by Balibar et al. [10]. This series nicely reveals the disappearance of three facets with increasing temperature. As the temperature increases the $(1\bar{1}01)$ or "s" facet roughens at $T_R^s \sim 0.35$ K followed by the $(1\bar{1}00)$ or "a" facet at $T_R^a \sim 1.0$ K and the (0001) or "c" facet at $T_R^c = 1.28$ K.

With the help of growth velocity experiments (see Chapter 6) Ballibar and coworkers were also able to determine the step free energy β/h of the (0001) surface of ^{4}He in the neighborhood of the roughening temperature [17]. The results are shown in fig. 5 and nicely follow the theoretically expected exponential temperature dependence of eq. 4.

Information on the universality class of the roughening transition may also be obtained from the thermal behavior of the rounded regions between the facets in the ECS. Below T_R, the facet edge at the boundary between the flat and the rounded parts should vary as [16]:

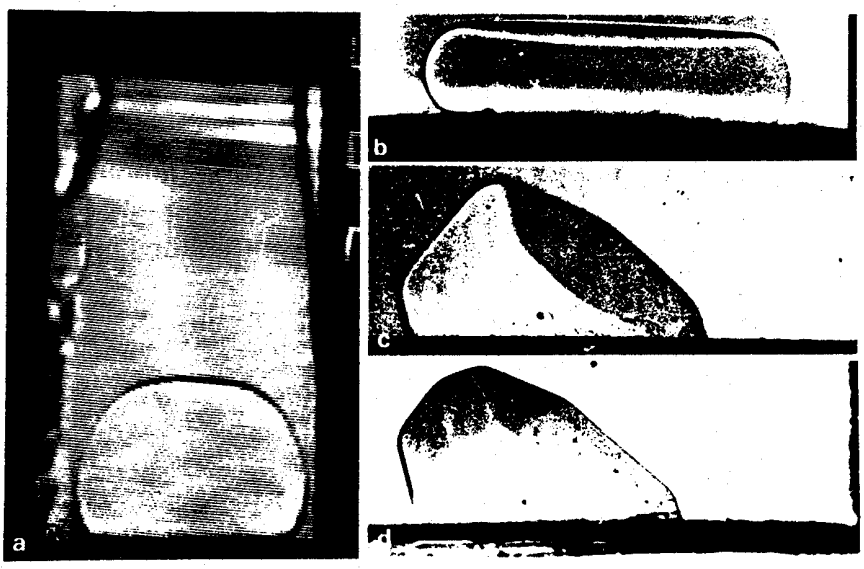

Figure 4. The development of new facets in helium-4 crystals upon lowering the temperature from 1.3 K (a) through 1.08 K (b), and 0.4 K (c) to 0.35 K (d) [10].

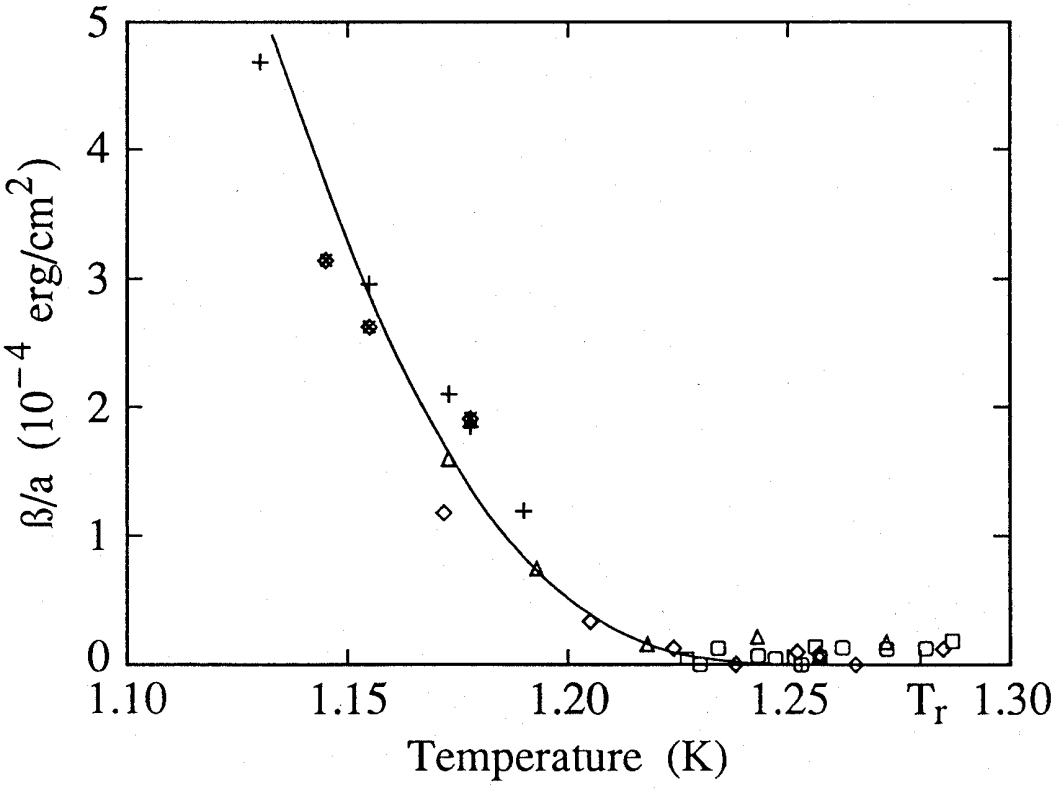

Figure 5. Temperature variation of the step free energy β/h on (0001) surfaces of solid ^{4}He close to their roughening temperature [17].

$$H \sim (r - r_0)^{\xi} \qquad (5)$$

where r_0 is the radius of the facet. Theoretically the exponent $\xi = 3/2$ has been predicted which is characteristic for the Pokrovsky-Talapov universality-class and should be independent of temperature and facet orientation for $T < T_R$. Experimental investigations of the ECS of small Pb and ^{4}He crystals are consistent with this prediction [18, 19]. A reexamination of the Pb-data concluded [20], however, that the data would also be in agreement with a mean-field exponent $\xi = 2$. More recent experiments with In-crystals [21], which tried to settle this question, were not successful because of a lack of accuracy in the determination of the profile origin (boundary between the facet and the rounded region).

3 DETECTION OF STEPS AT SURFACES

3.1 Surface microscopy

Very attractive techniques to detect monatomic steps on surfaces are direct imaging methods like field ion microscopy (FIM) [22], low energy electron microscopy (LEEM) [23] and scanning tunneling microscopy (STM) [24]. FIM provides atomic resolution but is restricted to the presence of high electric fields and in particular to small areas. Only local defect structures can be detected.

LEEM, which uses diffracted electrons to image surfaces is particularly suited to study step arrangements on mesoscopic length scales, its current lateral resolution limit of 200 Å does however not allow the resolution of atomic details.

The most powerful tool to study defects at surfaces is certainly the scanning tunneling microscope. It provides direct, real-space images of the surface topography on the atomic scale. In a typical constant-current topography scan a surface step is easily identified as a vertical movement of the tip by one lattice spacing. The step structure (kinks) and orientation are easily determined. In fig. 6 and we show two examples [25].

Fig. 6a shows an STM-topograph image of a well-prepared and annealed Pt(111) surface. The large-scale image reveals extended flat terraces separated by monatomic steps, with average terrace widths exceeding 2000 Å. The monatomic steps of height $h = 2.27$ Å have a very low density of kinks and run straight in the $[1\bar{1}0]$ direction.

In fig. 6b a smaller area STM image shows the step-terrace topography of a Pt (997) surface. This is a vicinal surface consisting of (111) terraces, separated by monatomic $[1\bar{1}1]$ steps $d = 20.2$ Å apart. The regularly spaced steps running along $[1\bar{1}0]$ are clearly visible. The kink density is found to be much higher in this case.

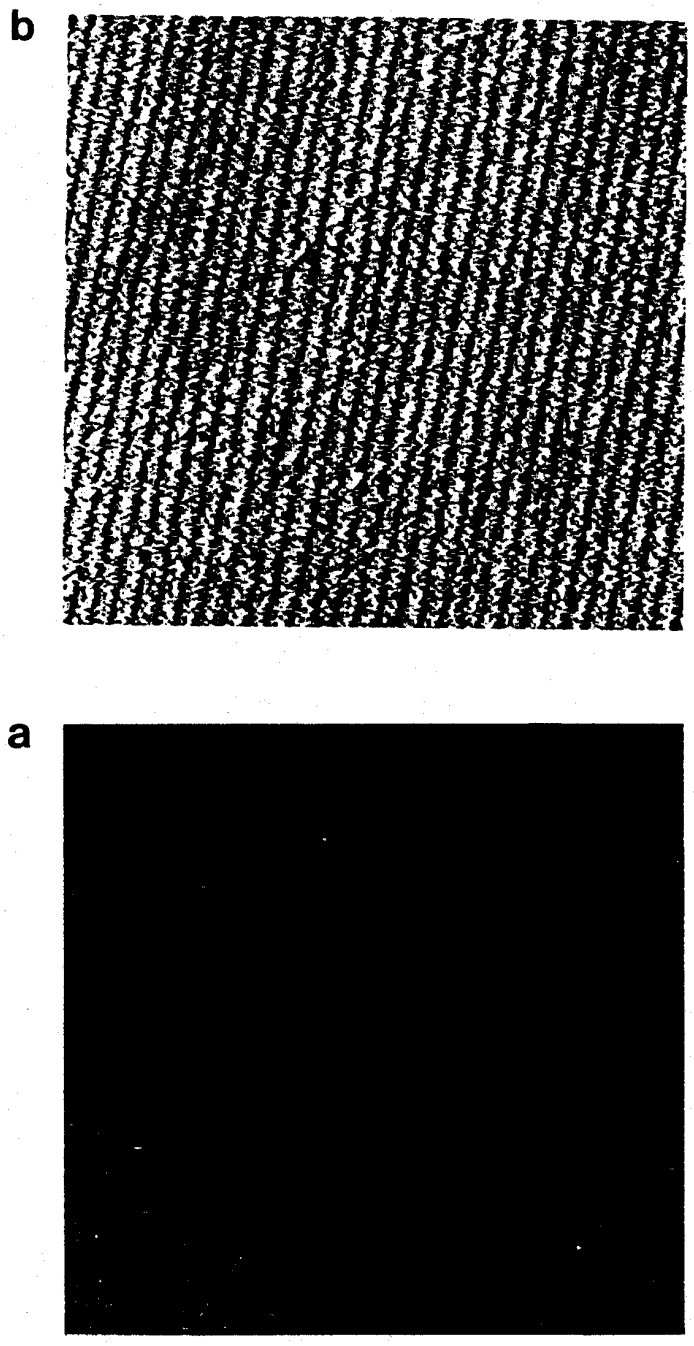

Figure 6. Scanning tunneling microscopy images of the close-packed Pt (111) (2000 Å × 2000 Å) (a) and the vicinal Pt (997) surface (600 Å × 600 Å) (b) [15].

These two examples nicely demonstrate the power of the STM in the study of surface defect structures. The technique has, however, also its limits. As a probe of step densities and distributions this limit is mainly given by the finite scan range which can be probed with sufficient resolution. In the case of point defects the STM may even give ambiguous results. Operated with lateral atomic resolution it will certainly detect a point defect, but may not necessarily be able to distinguish a vacancy from an adatom.

3.2 Surface diffraction

3.2.1 Diffraction peak width and height. The classic technique for the analysis of defect structures on surfaces is certainly diffraction (LEED [26], X-ray diffraction [27], He-diffraction [28]). The observed diffraction pattern in reciprocal space can be described as a Fourier transform of the surface atom arrangement. Because only intensities and no phases are measured in the diffraction experiment, the Fourier transform cannot, however, reversed directly to the actual atomic structure. Several schemes have been developed to overcome this problem and to extract atomic coordinates from measured diffraction intensities. A qualitative analysis of surface imperfections is, however, possible just by visual inspection of a diffraction pattern [29]. Intensity and shape of a diffraction spot are changed in a characteristic way by the appearance of certain surface defects. In the following we will give a short introduction into the analysis of surface defects by a quantitative examination of diffraction spot shapes (height, width, lineshape).

We will begin our discussion with the influence of thermal disordering and point defects (adatoms or vacancies). The characteristic wave-length of these defects are of the order of atomic dimensions and much smaller than typical domain sizes of ordered surface regions. Thus, the Fourier components describing displacements due to thermal vibrations and point defects have wave-lengths of atomic dimensions and the net effect is the appearance of a diffuse background intensity that reduces the intensity of the diffraction rods, but causes no broadening. In a first order approximation the diffracted intensity from a perfect single crystal surface drops exponentially with temperature and point defect density [30]:

$$I \sim \exp\left[-\langle (Q\,u)^2 \rangle\right] \cdot (1-\theta)^{n_s \cdot \Sigma} \qquad (6)$$

here Q is the momentum transfer, u the mean square displacement of the surface atoms, n_s the number of surface lattice sites, Σ the cross section for diffuse scattering from isolated defects and θ the point defect concentration.

Of particular concern for surface roughening studies are the influence of steps on the diffraction pattern. As a first example we will discuss the diffraction pattern of a vicinal surface, i.e. the diffraction from a regular monotonous step array [31]. The reciprocal lattice of a vicinal surface (fig. 7) is given by the product of the terrace structure factor (periodicity a) and the reciprocal lattice associated with the macroscopic surface (step periodicity d),

i.e. is a convolution of the single terrace unit with the step lattice. The reciprocal step lattice (infinite dimensions) has sharp rods which are inclined with respect to the diffraction rods associated with the terraces. The later are broad due to the finite dimensions of each terrace.

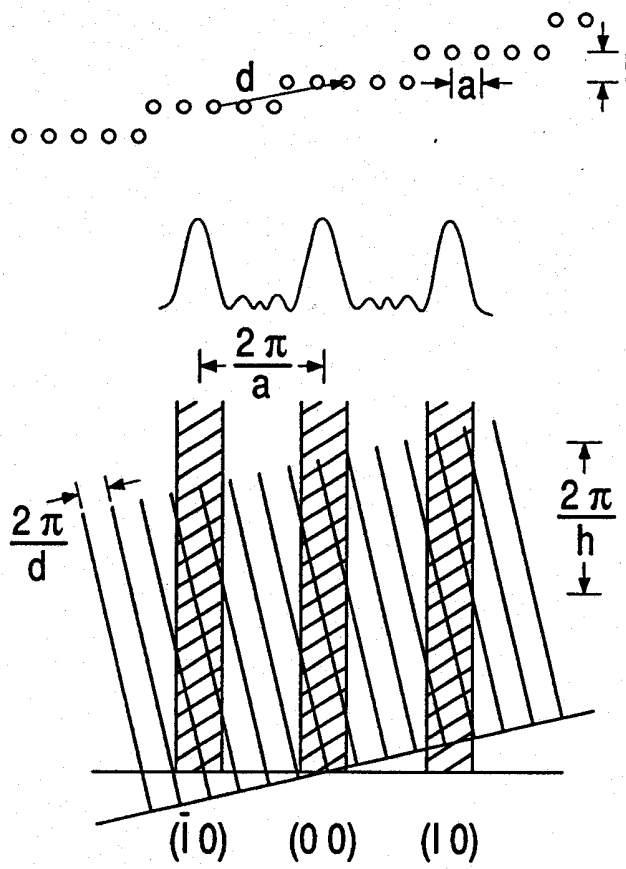

Figure 7. Schematic illustration of the diffraction from a regularly steeped surface. The complete reciprocal lattice is a convolution of the terrace- and the step-lattice-structure-function [31].

The schematic reciprocal lattice of random step arrays is shown in fig. 8 [29], for a two layer system and a many layer system, respectively. We will begin with the discussion of random steps in only two layers. The reciprocal lattice of such a surface consists of rods modulated in $Q_\perp$ that are not inclined, because the average surface is flat. The oscillation in $Q_\perp$ is determined by the step height h and can be explained by the interference of waves diffracted from the upper and lower terraces. If the interference is constructive or in-phase (i.e. the phase between the two waves is an even multiple of π), the diffraction is identical to that of the ideal step free surface with sharp peaks at $2\pi n/a$ ($n = 0, 1, 2, ...$). For the case of destructive interference or anti-phase diffraction (i.e. the phase between the two waves is an odd multiple of π), however, the sharp central peaks at $2\pi n/a$ (diminished in

intensity) are surrounded by a peak doublet of maximum intensity and spacing $2\,\pi/L$, where L is the average distance between terraces of equal height. The sharpness of this second feature is strongly dependent on the exact distribution of terrace sizes. In extreme cases it can degenerate to one single broad feature of width $2\,\pi/L$.

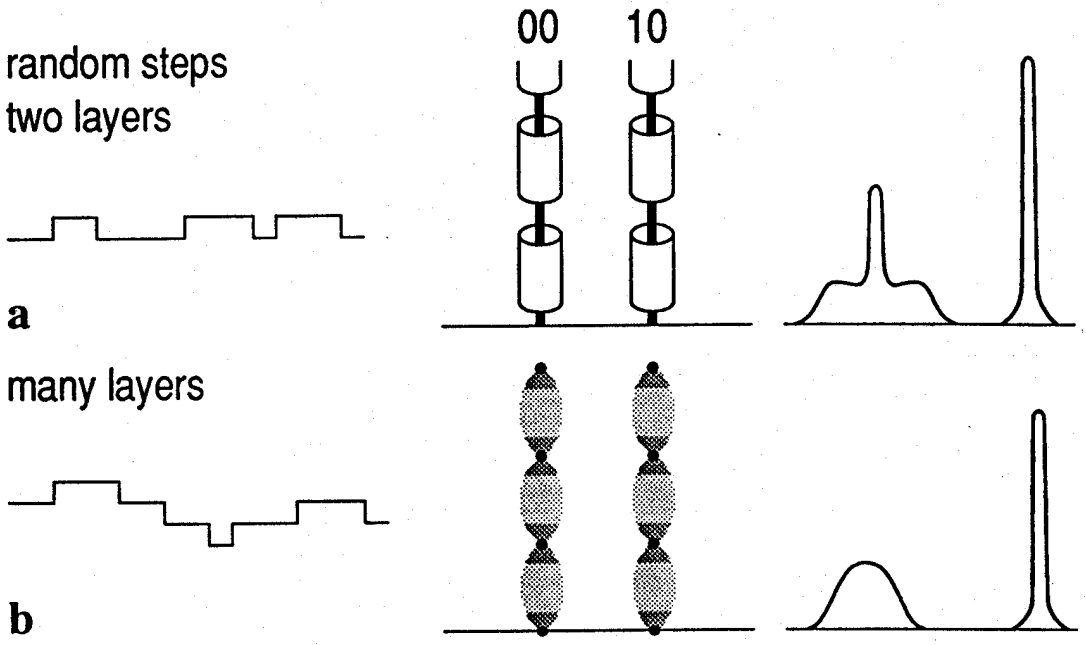

Figure 8. Diffraction signatures from random step arrays [29].

Random step arrangements distributed over many layers are again characterized by in-phase – anti-phase oscillations along $Q_\perp$. At the conditions for which all the terraces scatter in phase, the diffraction spots are sharp. At all other values of $Q_\perp$ they will be broadened and the broadening will have a maximum in anti-phase condition. The anti-phase peak-width is a direct measure of the average step density and the oscillatory period along $Q_\perp$ reflects again the step height.

In some favorable situations monatomic steps can also give rise to shifted (in $Q_{||}$) diffraction peaks, and the step density can be extracted directly from the peak shift [32]. Such a case is discussed in chapter 4.2.

In figs. 9 and 10 we show two experimental results demonstrating the in-phase – anti-phase oscillations of randomly stepped surfaces. The first example is a He-diffraction study of the Pt (111) surface which was artificially roughened with Ar-ion bombardment [33]. Plotted in the graph is the specular He-beam intensity, normalized to the incident beam, as a function of the angle of incidence $\vartheta_f = \vartheta_i$ (i.e. a measure of $Q_\perp$). Curve a), which characterizes the artificially roughened surface, shows the expected oscillatory behavior. The minima and maxima correspond to anti-phase (↓) and in-phase (↑) scattering geometry. The periodicity of the oscillations is consistent with

the presence of monatomic steps of height $h = 2.27 \pm 0.05$ Å and the amplitude of the oscillations yield an average terrace width of ~ 100 Å. Curve b) which characterizes a much smoother Pt (111) surface with average terrace widths of ~ 2000 Å (compare with the STM image in fig. 6 characterizing a Pt (111) surface of similar quality) shows no oscillations at al. The observed intensity increase with increasing momentum transfer reflects the expected Debye-Waller behavior (eq. 6). The absence of oscillations in fig. 9 a) is related to the finite resolution of the He-diffractometer. Quite general each diffraction experiment is limited in the analysis by its maximum instrumental resolution in momentum space. A convenient measure of this instrumental resolution is the so-called transfer width ω [30]. The transfer width can be associated with a length at the surface, which would lead to the instrumental width of the diffraction peaks. It represents the linear scale at which information on the surface periodicity can be obtained directly [30,31]. The value of ω is determined by the angular openings of beam and detector and the monochromaticity of the diffracting wave and ranges from 100-200 Å (standard LEED) over 200-1000 Å (He-diffraction) to 100-10'000 Å (gracing incidence synchrotron X-ray diffraction). With the help of deconvolution the largest average terrace widths which can be detected are about 10 ω. The absence of any oscillatory behavior in the specular He intensity in fig. 9 b) determines the average terrace width to be larger than 10 $\omega \approx$ 2000 Å, in nice agreement with the STM-image in fig. 6.

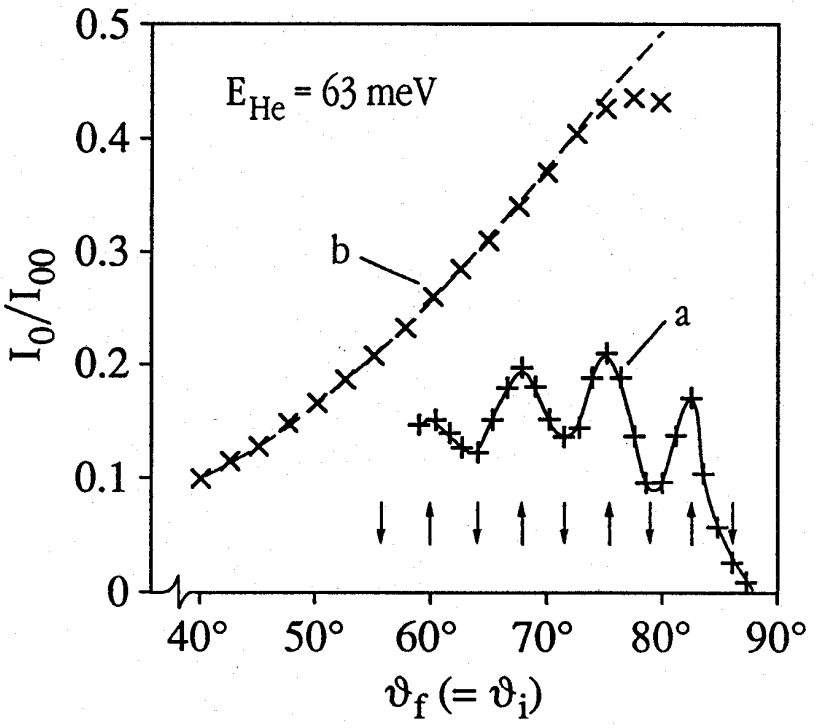

Figure 9. Specularly reflected He-intensity from Pt (111) as a function of incidence angle. The two-curves correspond to a well prepared sample (b) and to an artificially roughened surface (a), respectively [33].

The second example demonstrates the generation of in-phase – anti-phase oscillations due to the thermal generation of steps, i.e. due to surface roughening. Fig. 10 shows the measured width of the specular electron diffraction peak from Pb (110) as a function of perpendicular momentum transfer at surface temperatures of 303 K and 475 K [34]. As the temperature is increased the peak width changes dramatically from a constant value at

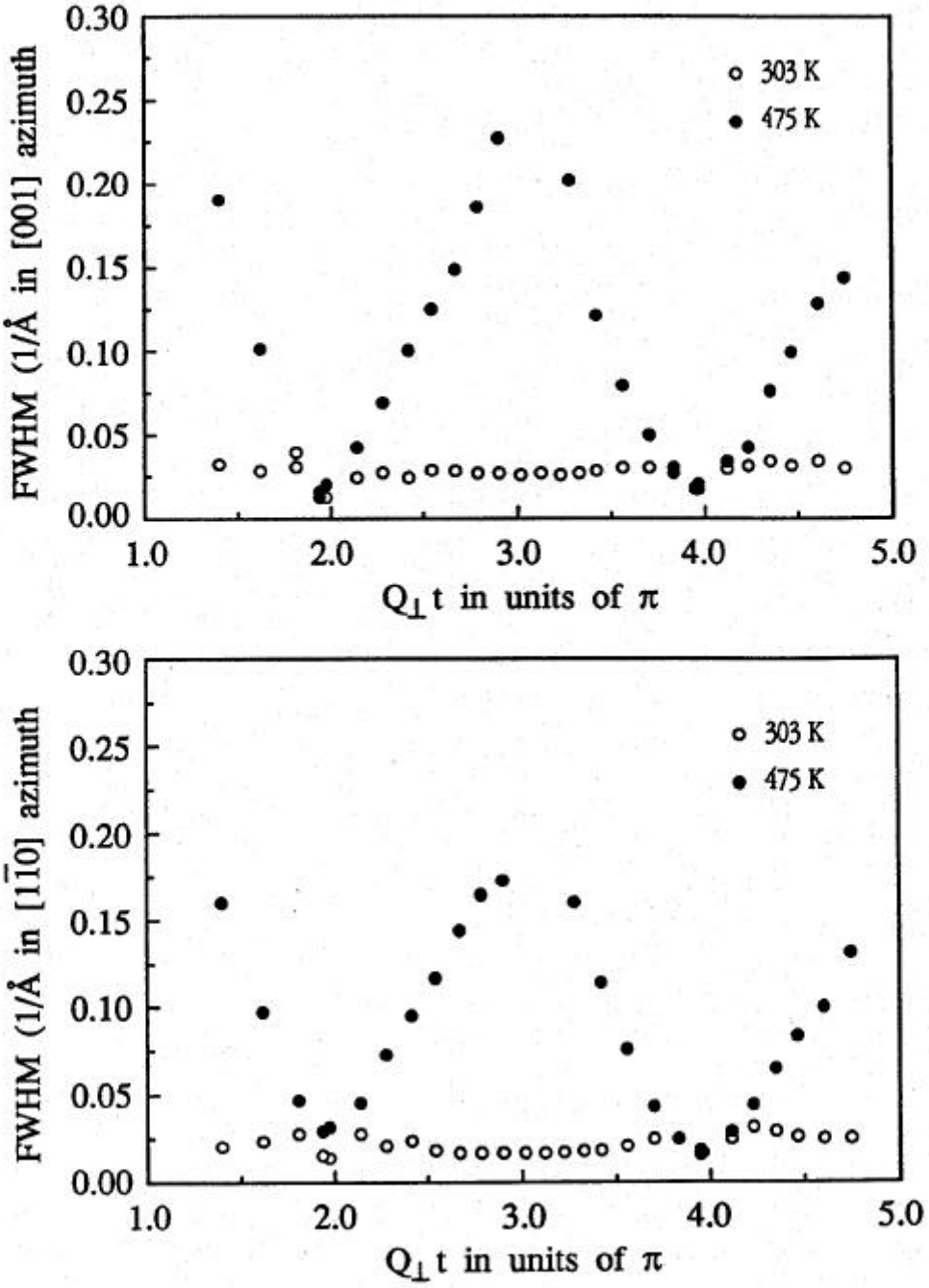

Figure 10. The diffraction peak-width of low-energy-electrons specularly reflected from the Pb (110) surface at 303 K and 475 K [34].

303 K to an oscillatory behavior at 475 K. The oscillations at high temperatures clearly demonstrate the proliferation of steps. From the period of the oscillations the presence of monatomic steps of height $h = 1.75 \pm 0.05$ Å is deduced. The terrace width is estimated to be around 35 Å with the help of the amplitude of the oscillations.

3.2.2 Diffraction line shapes. In the above paragraph we have seen that the visual observation of diffraction spots allows a qualitative analysis of surface defect structures. In particular the measured intensities and peak widths as a function of momentum transfer can be used to deduce the average step height and the average step density. With a simple analysis of intensity and width it is, however, impossible to evaluate the actual distribution of surface defects quantitatively.

It is however just the quantitative distribution function of steps, which distinguishes a thermally roughened surface from an artificially roughened surface. The basic characteristic of the surface roughening transition is the logarithmic divergence of the height-height correlation function above T_R. At temperatures $T < T_R$ the height-height correlation function $g_\perp(r)$ remains bounded, while for $T > T_R$, resulting from the spontaneous proliferation of monatomic steps, $g_\perp(r)$ diverges [9]:

$$\lim_{r \to \infty} g_\perp(r) \propto \begin{cases} R(T) = \text{const} & \text{for } T < T_R \\ C(T) \ln(r) & \text{for } T \geq T_R \end{cases} \tag{7}$$

This pair correlation function reflects directly in the line shape of the diffraction peak. Within the kinematical approximation the measured line shape is given by the convolution of the lattice factor $G = \sum_{ij} \exp[-i Q (r_i - r_j)]$ and the instrumental response factor $T(Q)$. Since the lattice function is the Fourier transform of the pair correlation function $g(r)$ the lineshape of a diffraction gives directly $g(r)$ upon deconvolution with the instrumental response function. In fig. 11 we show some height-height pair correlation functions corresponding to different kinds of rough surfaces and the resulting diffraction peak line shapes [27].

Fig. 11 a) has a linear divergence of $g_\perp(r)$ giving rise to a Lorentzian lineshape. The width of the diffraction line is proportional to the slope of $g_\perp(r)$. In fig. 11 b) the case of a stochastically rough surface with no divergence is shown, i.e. on all distances there is a certain finite random rms height variation h_{rms} resulting in $g_\perp(r) = 2\, h_{rms}$. The resulting diffraction peak is a delta-function in $Q_\parallel$. In the intermediate case c) $g_\perp(r)$ is constant at large distances, while the linear increase for small r is associated with local steps. The corresponding line shape is a two-component composite of a) and b). The correlation function in graph d) finally illustrates the thermal

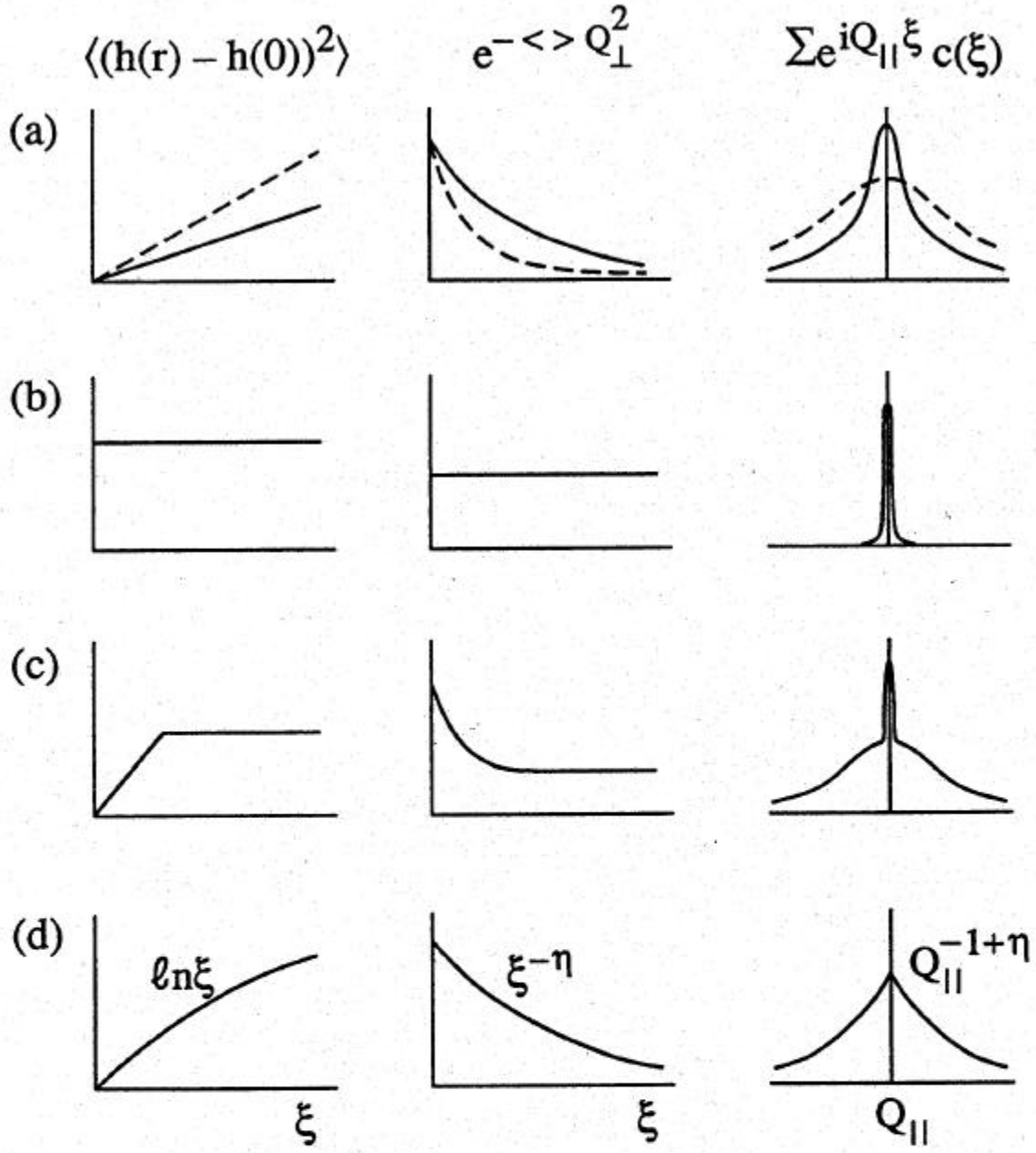

Figure 11. Different height-height correlation functions of various rough surfaces and the resulting diffraction line shapes [27].

roughening scenario with logarithmic height divergence. The diffraction line shape has the characteristic power-law form [35]:

$$I(Q_{\parallel}, Q_{\perp}) \propto \frac{1}{\sin^2(Q_{\perp}/2)} \; Q_{\parallel}^{-(2-\tau)} \tag{8}$$

$Q_{\parallel}$ and $Q_{\perp}$ being the parallel and perpendicular momentum transfer, respectively and τ the so-called roughness exponent

$$\tau = \frac{\pi}{2} K(T)\, f(p) \qquad (9)$$

K (T) is the so-called roughness parameter. Everywhere in the low temperature phase the effective K (T) is equal to zero (no power law line shape); at the roughening transition it jumps to the universal value $K(T_R) = 2/\pi$ (see e.g. ref. 35), and increases with temperature continuously in the rough phase. The function f (p) describes the scattering kinematics and varies from $f(p) = 0$ for in-phase diffraction to $f(p) = 1$ in anti-phase geometry. Theoretically f (p) varies with the model and also depends on finite size effects, from a (periodically repeated) square to a simple cosine function of the phase p. Thus, at the roughening temperature in a perfect anti-phase diffraction experiment we have $\tau_R = 1$.

In chapters 4 and 5 we will discuss several experimental examples which make use of the diffraction line shape analysis to detect the surface roughening transition.

4 ROUGHENING OF NONVICINAL SURFACES

4.1 Nonreconstructed fcc (110) surfaces

Particularly attractive for roughening studies of low index metal surfaces are (110) surfaces of fcc-crystals. Firstly, the (110) surface has the most open structure of the three densest fcc-faces, (111), (100) and (110); resembling to some extent the topography of the vicinal (113) surface. The second aspect is surface reconstruction. The (110) surfaces of transition metals with face centered cubic (fcc) symmetry belong to two different classes. The first class, including the 3d-elements Cu, Ni and the 4d-elements Rh, Pd and Ag, have a nonreconstructed (1×1) ground state for the clean surface, i.e. they keep the bulk termination (they exhibit however large oscillatory interlayer-relaxations). The second class of fcc metals, including the 5d-elements Ir, Pt and Au, exhibits a reconstructed (1×2) ground state. The nature of the (1×2) reconstruction has been studied extensively by a number of different experimental techniques and there is a general agreement now that the (1×2) phase of all three 5d-metals is a missing row geometry [36] with every second close packed [1$\bar{1}$0] row missing (see fig. 12).

It was suggested that reconstruction and roughening in these systems are indeed related [37]. As pointed out by Garofalo et al. the energies of the relaxed unreconstructed (1×1) surface and the energies for all possible missing-row states (1×2, 1×3, ..., 1×4), are all energetically close to one another [38]. Locally the (1×n) reconstructions represent microscopic (111) facets and are expected to be easily excitable at elevated temperatures. Trayanov et al. [37] speculate, that whatever the low-temperature ground state configuration (unreconstructed or reconstructed) it might roughen into a high temperature disordered phase, with a mixture of (1×n) configurations.

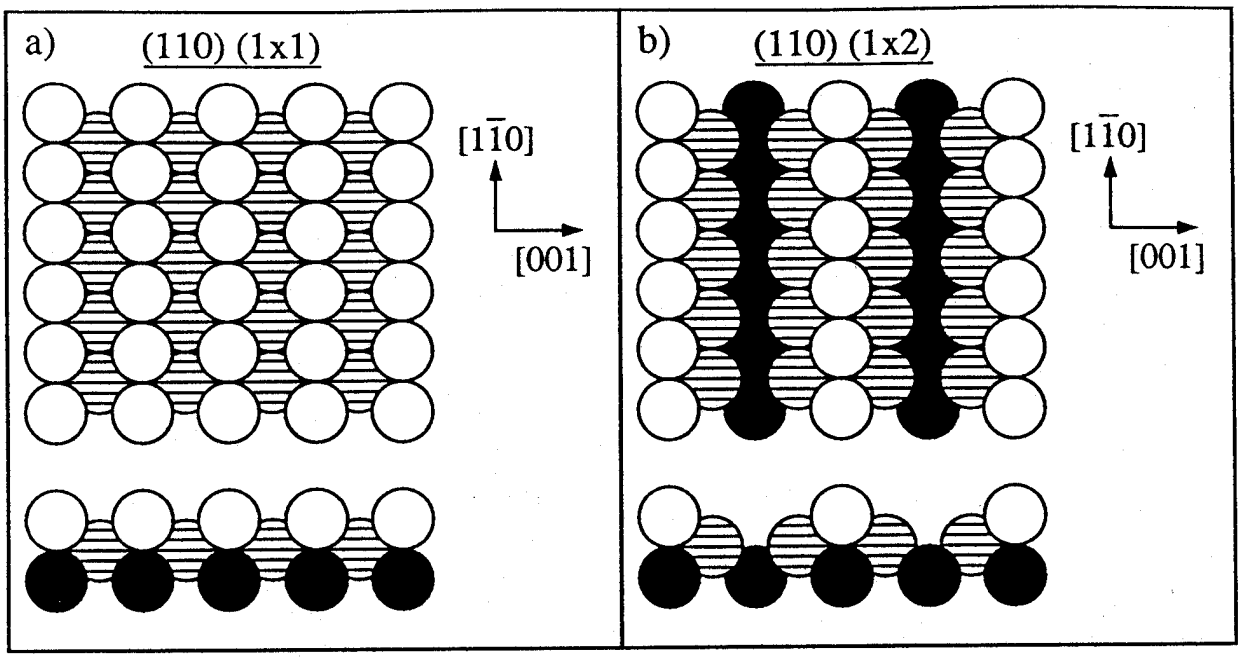

Figure 12. Structure of the unreconstructed and reconstructed (110) surface of face centered cubic metals.

4.1.1 The precursors to surface roughening : vibrational disordering and adatom-vacancy creation. More than fifteen years ago it had been noticed that the intensities in the photoemission spectra taken from Cu (110) decrease dramatically with temperature above ~ 500 K [39]. Similar effects have been seen recently in low energy ion scattering [40], in X-ray diffraction [41] and in thermal He scattering [42,43]. The dramatic intensity decrease observed in all cases above 450-500 K could not be accounted for by simple Debye-Waller effects. While Lapujoulade et al. [43] and Fauster et al. [40] proposed as explanation either anharmonic effects or some kind of disorder, Mochrie [41] concluded categorically – without qualitative additional evidence – that he was observing the roughening transition. He even tentatively identified the temperature at which "the intensity has fallen essentially to zero" (870 K) with T_R. A He specular intensity measurement on Cu(110) versus temperature of Zeppenfeld et al. [42] shows (fig. 13a) that also above 870 K the intensity continues to drop (at 1000 K it is already one order of magnitude lower) and that there is no sign of saturation even above 1000 K. Whether the intensity becomes "essentially zero" appears to depend on the dynamical range of the instrument, and is not a criterion for the choice of value of T_R. Zeppenfeld et al. have analyzed in detail the energy and angular distribution of the scattered He atoms in the whole temperature range up to 1000 K [41]. Recently Kern et al. extended these measurements up to 1100 K [44]. The analysis of the specular He-diffraction peak measured

in near antiphase-scattering geometry reveals the onset of step proliferation to be located at T_R = 1070 K, 200 K higher then estimated by Mochrie.

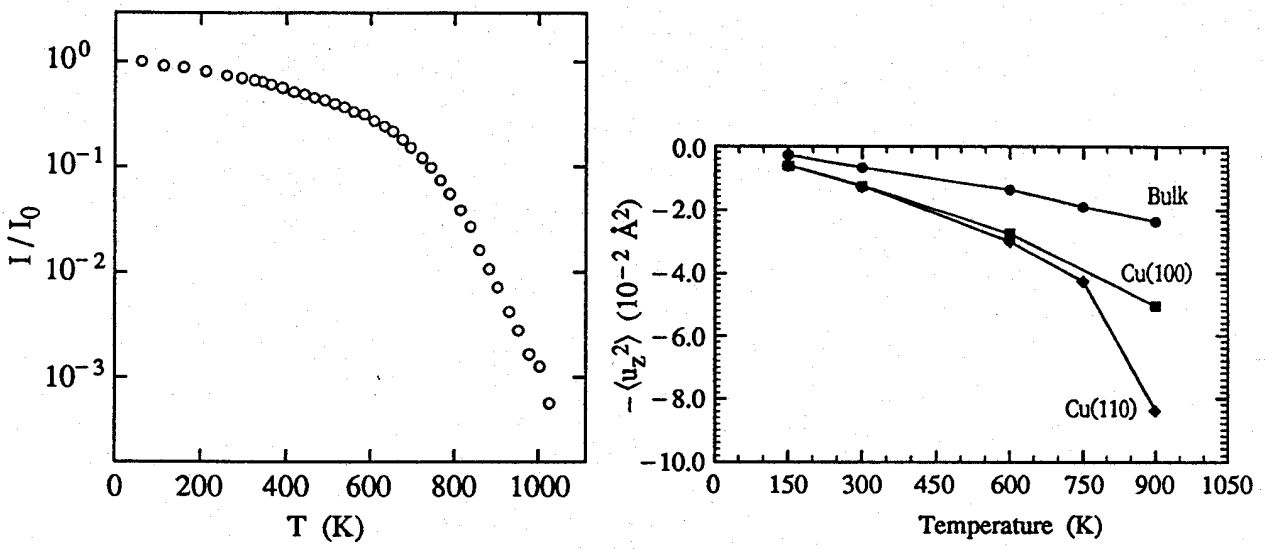

Figure 13. a) Thermal dependence of the He-specular peak height from Cu (110); He beam energy 18.3 meV and angle of incidence 45° [42]. b) Mean square displacements of surface atoms versus temperature [45],

It is generally accepted now that the surface roughening is preceded by two precursors : the onset of dynamical disorder through enhanced anharmonicity and the onset of static disorder through adatom-vacancy creation. In particular the sharp decrease in coherently scattered intensity above 0.35 T_M is ascribed to an anomalous large increase of the mean-square displacement of the surface atoms $< u_z^2 >$ due to a large anharmonicity in the metal potential at the surface. In fig. 23b we show the mean-square displacements $< u_z^2 >$ at the Cu(110) surface which have been deduced from the fitting of the measured temperature dependence of its surface phonon frequencies and widths [45].

An enhanced surface anharmonicity on the open (110) surface of fcc metal crystals has been deduced also from theoretical [46] as well as experimental [47] studies of the thermal surface expansion coefficient. Non-reconstructed fcc (110) surfaces are strongly relaxed and the interlayer distance between the first and second plane of atoms d_{12} is contracted between 5 and 15% with respect to the bulk value d_b. This relaxation was found to vanish rapidly above $\sim 0.4\ T_M$ (i.e. $d_{12}/d_b \rightarrow 1$) which can only be ascribed to a substantial increase of the thermal surface expansion coefficient driven by a strong surface anharmonicity. The corresponding experimental graph for Pb(110) is given in fig. 14.

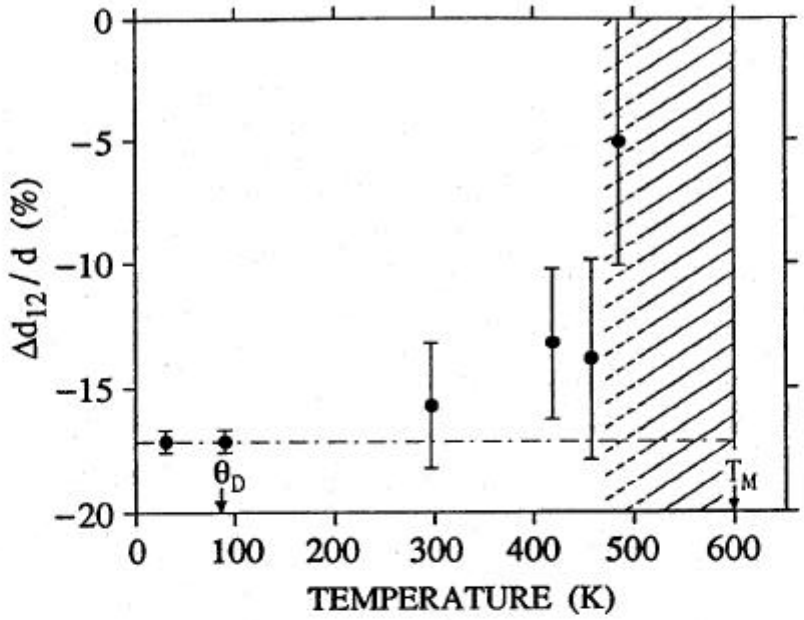

Figure 14. Surface relaxation of Pb (110) versus temperature [47].

The increase of $< u_z^2 >$ is however not sufficient to fully explain the substantial decrease of the coherent He-intensity in fig. 13a. In particular above 800 K the dynamic disorder is to small to account fully for the dramatic intensity decay. This temperature marks indeed the onset of adatom-vacancy creation. The defect concentration can be deduced from the specular He-intensity data, assuming that the decay is induced by dynamic as well as static disorder, using the $< u_z^2 >$ values of fig. 13b. In a simple Debye-Waller model with the assumption of a random distribution of additional adatoms and vacancies the attenuation of the specular He-beam I/I_o is given by eq. (6).

With this simple model and a value of $\Sigma \approx 70$ Å for the diffuse scattering cross section from isolated defects we estimate the concentration of isolated defects to be a few percent at 900 K. The deduced onset of adatom-vacancy creation around 800 K and their concentration is in nice agreement with recent molecular dynamics simulations of Hakkinen and Manninen [48], and ion scattering experiments of Dürr et al [49].

4.1.2 Thermal roughening of fcc (110) (1×1) surfaces. The observation of a surface roughening transition on the (110) faces of Ni and Pb was reported recently by Cao and Conrad [50] and by Yang et al. [34], respectively. Using high resolution LEED these authors showed the onset of step proliferation at $\sim 0.75\ T_M$. The roughening transition is preceded by two stages, a large increase of the mean square displacements of the surface atoms due to excess surface anharmonicity starting at $\sim 0.45\ T_M$ followed by adatom and vacancy creation above $\sim 0.7\ T_M$.

A detailed analysis of the Ni (110) LEED angular diffraction profiles by Cao and Conrad reveal a Gaussian central peak superimposed on a broad Lorentzian, which is interpreted in a two-level model. In this model the ratio of the Gaussian to the Lorentzian intensity is proportional to the adatom concentration, the width of the Lorentzian component characterizes the average step density. In fig. 15 the temperature dependence of these quantities as measured by Cao and Conrad is shown. The onset of adatom creation around 1150 K and the proliferation of steps around 1300 K (= 0.75 T_M) are evident. This behavior of the diffraction line-shape may however also be consistent with a preroughening-transition of the type discussed by den Nijs [51]. In the preroughening scenario steps are created spontaneously at the transition, but each step up is followed by a step down and vice versa and the surface remains flat on a macroscopic length scale.

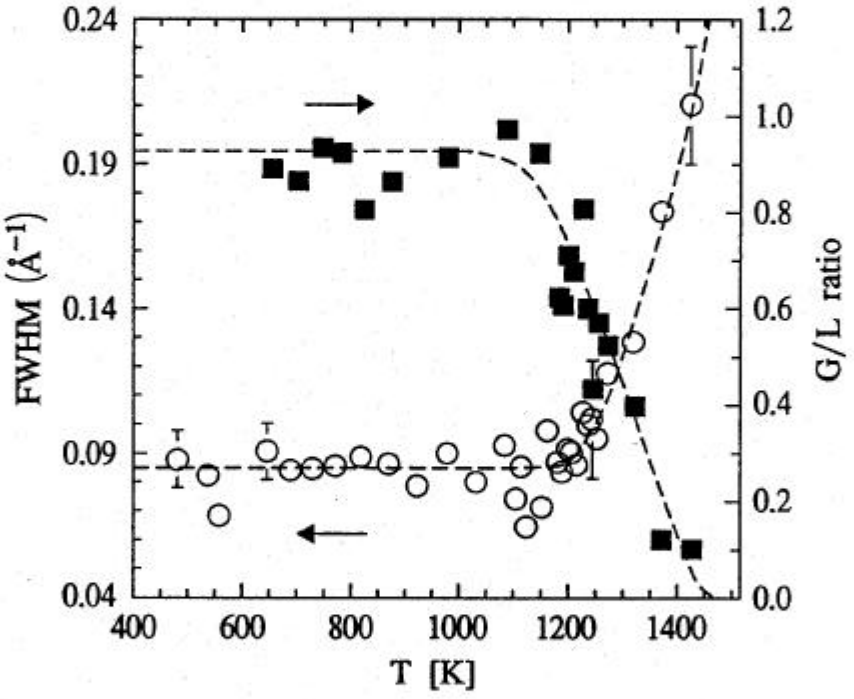

Figure 15. The ratio of the Gaussian to Lorentzian intensity (■) and the Lorentzian FWHM (○) of the specular anti-phase LEED diffraction peak from Ni (110) vs. temperature [50].

While the roughening of Ni (110) has been deduced from the broadening of the anti-phase Bragg peak, in the case of Pb (110) [34] the logarithmic divergence of the height-height correlation function was demonstrated. Figure 16 a) and b) show the thermal evolution of the zero order diffraction line shapes and the extracted roughening exponents τ_R and diffraction peak widths (FWHM) of the Pb (110) surface measured by low energy electron

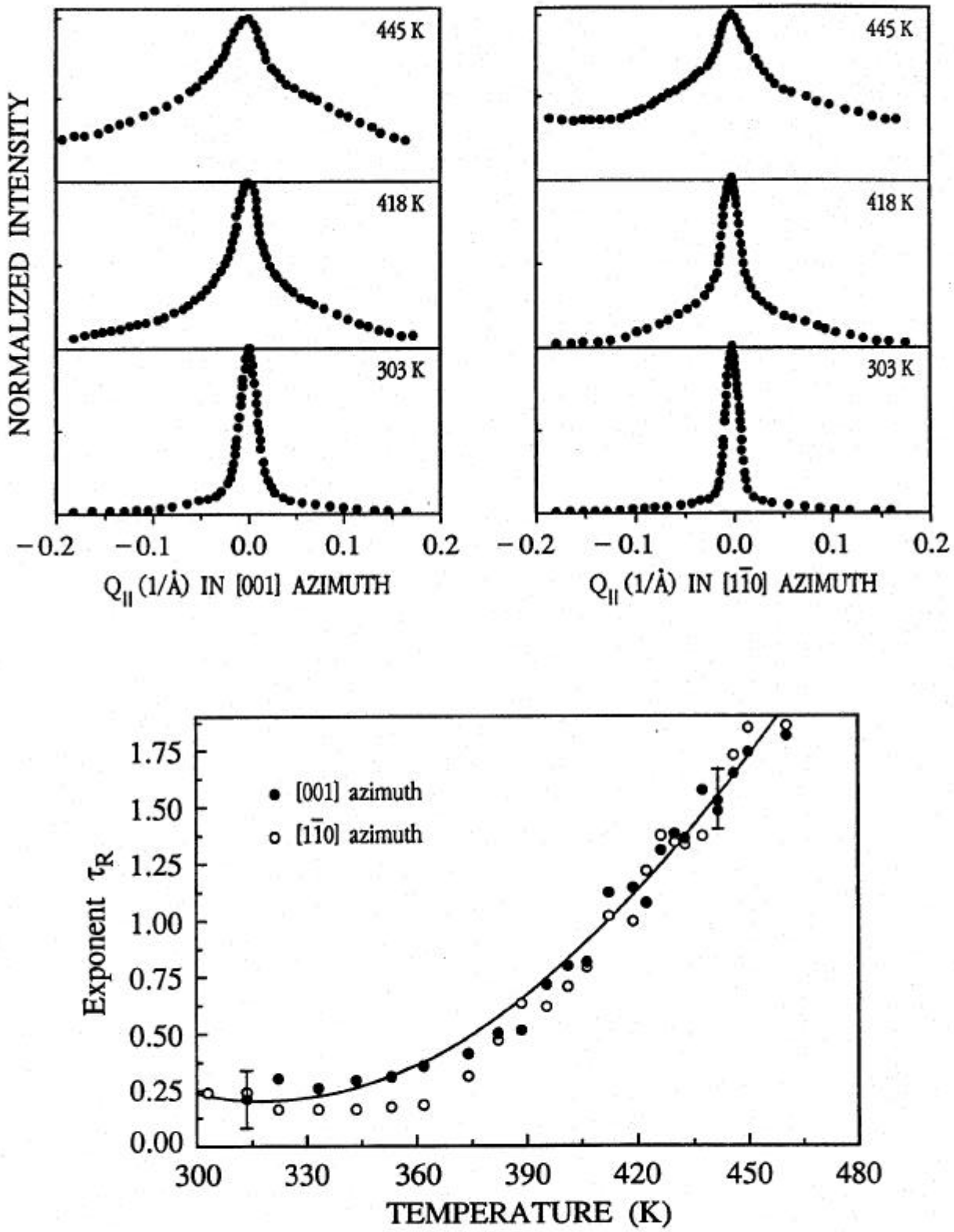

Figure 16. Diffraction lineshape (a) and extracted roughening exponent τ_R (b) of specularly from Pb (110) reflected low-energy electrons. The scattering geometry was selected to be in anti-phase [34].

diffraction. Measurements were taken along the [001] and [1$\bar{1}$0] directions with a beam energy of 27 eV in shear anti-phase scattering geometry. The line shape is sharp at low temperatures and develops a substantial tail at elevated temperatures. The measured diffraction line shape is found to be nicely fitted by eq. (8) indicating a logarithmic divergence in the height-height correlation function $g_\perp(r)$. The roughening temperature is determined to be $T_R = 415$ K, where the roughening exponent becomes $\tau_R = 1$. The corresponding peak-width increase at T_R appears to be asymmetric with a substantial broadening of $\sim 100\%$ for diffraction along the [001] azimuth and a much smaller broadening of only $\sim 30\%$ along the (1$\bar{1}$0) azimuth.

This observation might be the manifestation of an anisotropic surface roughening. The (110) surfaces of fcc metals exhibit anisotropic surface properties. The free energy of steps running along [100] is supposed to be quite different from that of steps running along the [110] azimuth, and because surface roughening depends on these energies it is expected to be anisotropic as well. This point was particularly stressed by Bonzel et al. [52] and Trayanov et al. [54]. The step configuration along the [100] direction is an open edge of the {100} type while along the [110] direction steps are of the close packed {111} type. The step free energy for the open {100} type is expected to be significantly higher than that of the close packed {111} step. For platinum surfaces the relation of these step free energies has recently been quantified [54] to be $\beta_{\{100\}} = 1.15 \pm 0.02\ \beta_{\{111\}}$ · {111} steps should thus be excited thermally at lower temperatures than {100} steps.

Bonzel et al. [52] suggest, based on X-ray photoelectron-diffraction data of Pb(110), that the transition observed by Yang et al. [34] is solely accounted for by the proliferation of {111} steps in the [110] azimuth. They identify this transition with the den Nijs preroughening transition [51] from the ordered flat (OF) to the disordered flat (DOF) surface. In their scenario the free energy of {100} steps vanishes only above 500 K, and because both step free energies $\beta_{\{111\}}$ and $\beta_{\{100\}}$ approach zero at T_R of the (110) surface the roughening temperature was suggested to be larger than 500 K. The model of Bonzel et al. is based on the analysis of temperature dependent XPD-data. In the forward scattering enhancement peak intensity versus temperature for Pb (110) they observe anomalies at ~ 360 K upon scattering along the [110] azimuth and at $\sim$ 500 K along the [100] azimuth. They attribute these anomalies to the onset of step proliferation of {111} and {100} steps, respectively.

In their argumentation Bonzel et al. [52] neglect, however, the observed diffraction line shape of Yang et al. [34] for the LEED-spot profiles. The observed power-law behavior according to eq. (8) clearly identifies a thermally rough surface with a logarithmic diverging height-height correlation function $g_\perp$ (r) above $T_R = 420$ K. Indeed, it is questionable, how a technique like XPD which is sensitive to short range order only, could be used to analyze long-range defect structures which are relevant to surface roughening. We recall here that at T_R the height fluctuation is only one

lattice spacing for a distance of 139 lattice spacings. It is more likely that the LEED-experiment of Yang et al. determines the correct roughening temperature of T_R = 420 K and that the observed asymmetry in the measured peak-widths reflects the anisotropic character of the roughening transi–tion. While the onset of broadening at 370 K along [100] marks the proliferation of {111} steps the delayed onset at 410 K along the [110] azimuth reflects the proliferation of energetically less favorable {100} steps.

From a detailed analysis of elastic He-diffraction profiles it was estimated [55] that Cu(110) may indeed roughen at similar relative temperatures (with respect to the bulk melting temperature). Extrapolating of the roughening exponent measured by Zeppenfeld et al. [42] the roughening temperature of Cu (110) was estimated to be $T_R \approx 1070$ K = 0.79 T_M. This roughening temperature was recently confirmed by measurements of the specular He peak-width in exact anti-phase geometry by the same group [44]. At 1070 K they measured the theoretically expected peak broadening of 60%. The intensities were to low, however, to perform a detailed line shape analysis with sufficient statistics.

That this value might indeed be the correct roughening temperature of Cu(110) is supported by diffusion measurements of Bonzel and coworkers [56–58]. These authors studied the surface self diffusion of various fcc (110) surfaces by monitoring the decay of a periodic surface profile. The profile with periodicities of a few μm is prepared by a photoresist masking technique and subsequent Argon RF-sputtering and the analysis of the profile decay at elevated temperatures is done by laser diffraction [56–58]. The results for Ni(110) and Cu(110) are plotted in fig. 17. Below the roughening temperature the macroscopic diffusion is expected to proceed by single adatom diffusion while above T_R the macroscopic mass transport should be dominated by meandering steps. Surface diffusion of adatoms on the (110) surface of fcc-crystals is expected to be anisotropic because of the two-fold symmetry of the surface. This expectation is confirmed by the data in fig. 17. At low temperatures the activation energy for diffusion along the close packed channels, i.e. along the [1$\bar{1}$0] direction, is found to be only 40% of the barrier for across channel diffusion, i.e. diffusion along the [100] azimuth. Above this temperature the mass transport is isotropic, consistent with two-dimensional step diffusion. We thus conclude that the diffusion data in Fig. 17 support a roughening transition of Ni and Cu (110) around 78% of the melting temperature.

Evidence for the roughening of the (110) surface has also been presented recently for the metals In [59], Ag [60] and Pd [61]. While the roughening of the [110] surface of In is generally accepted, the experimental results for Ag(110) and in particular Pd(110) are disputed. For palladium Francis and Richardson [61] reported an order-disorder transition to occur around 250 K. This transition was, however, not be detected in a series of subsequent experiments [62] and today is believed to be an artifact due to the presence of impurities in the experiments of Francis and Richardson.

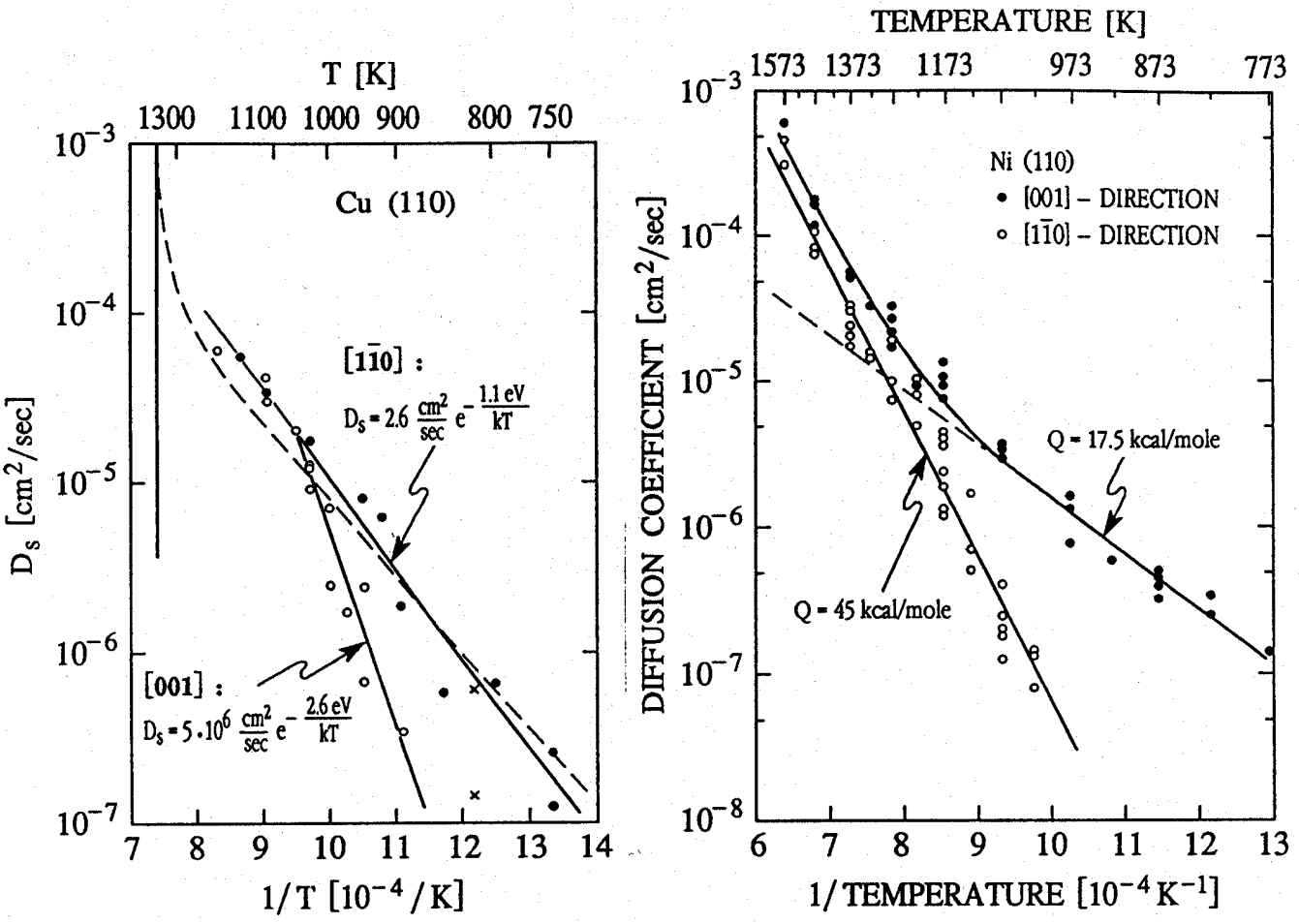

Figure17. Arrhenius plot of the surface self-diffusion coefficient for Ni (110) and Cu (110) [56–58].

Ag (110) is an interesting case. This surface was studied by Held et al. [60] with synchrotron x-ray diffraction. Based on a diffraction peak shape analysis they deduced the relatively low roughening temperature of 0.56 T_M. Robinson et al. [63] recently repeated the x-ray measurements on Ag(110) and came to a surpri–sing result. They demonstrated that the Ag(110) surface below its roughening temperature coexists of flat (110) oriented regions and slightly inclined, rough regions. Thermal roughening takes place by the gradual replacement of the (110) faceted regions by the rough phase and the roughening temperature depends substantially on the misorientation of the crystal surface.

In fig. 18 we show the measured inclination angle between the flat and the rough regions on the surface. At about 790 K the tilt angle becomes a constant ($\alpha_o = 0.14°$) which agrees with the known miscut of the sample. The roughening temperature of the perfect (110) surface is found by extrapolating to the temperature where α (T) = 0, giving a value of $T_R \approx 990$ K = 0.80 T_M.

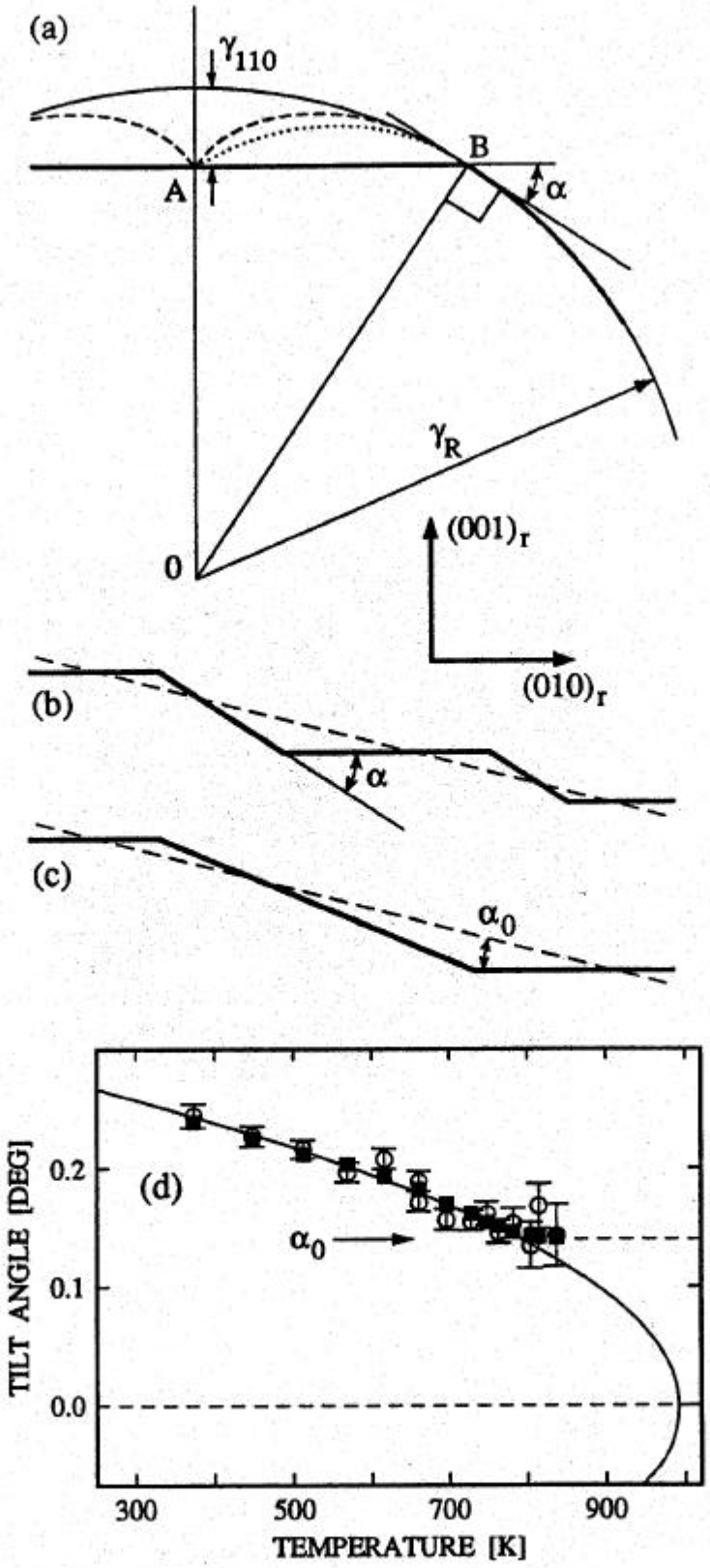

Figure 18. a) Wulff construction of the ECS (thick line) containing a flat facet with a sharp edge. b) and c) illustrate the resulting hill and valley morphology for different values of the surface free energy γ_{110} (T) [65]. d) Measured tilt angle between the rough and the flat regions of the Ag (110) surface vs. temperature [63].

The phase coexistence of large flat regions with inclined highly stepped regions has been observed recently by STM for several "soft" metal surfaces namely Ag(111) misoriented by 1.6° towards the [2$\bar{1}\bar{1}$] direction, Cu (100) and various vicinal Cu(11n) surfaces [64–66]. In fig. 19 we show as an example the STM-topograph image of the misoriented Ag(111) surface. The image reveals a faceted surface with about 1000 Å wide flat (111) terraces separated by a 300–400 Å wide stripe with a high density of steps. The steps are spaced 10–50 Å apart and run preferentially along the [110] directions. The highly stepped region is inclined by about 5° with respect to the flat (111) terraces.

Figure 19. Scanning tunneling microscopy image (2200 × 2200 Å2) of a 5° misoriented Ag (111) surface [66].

The observation of phase coexistence can be understand in the frame-work of the theory of the ECS. As long as isolated steps can exist on the surface all vicinal directions close to the low-index surface are stable. If isolated steps are, however, unstable with respect to congregalation, most vicinal surfaces close to the low index facet become forbidden. This is illustrated in fig. 20. Microscopically, the step-congregalation is caused by attractive medium-range step-step interactions. The attractive character of step-step interactions at intermediate distances of 10–20 Å was recently verified by Frohn et al. [65] in an STM-investigation of the terrace-width distribution for the nominally flat Cu(100) surface and (11n) vicinals. The measured distance distribution of two adjacent steps revealed always a

maximum at 11,5 Å independent of the nominal average step distance, varying from 9 Å to 25 Å.

In summary, the experimental data for all nonreconstructed fcc (110) surfaces clearly favour the occurence of a roughening transition at temperatures of ~ 70% to 80% of the bulk melting point. The measured roughening temperatures are collected in table I.

TABLE 1
The roughening temperatures of fcc(110) (1 × 1) metal surfaces.

Surface	T_R [K]	T_R/T_M	References
In(110)*	290	0.69	59
Pb(110)	420	0.70	34, 67
Ag(110)	990	0.80	63
Ni(110)	1300	0.76	50
Cu(110)	1070	0.79	44, 55
*tetragonal			

Upon further increase of the temperature the nonrestructured (110) surfaces may start to melt well below the bulk melting temperature T_M. A disordered liquid surface layer can emerge which would grow in thickness as $T \rightarrow T_M$. The undercooled liquid layer which is intercalated between the vapor and the solid can then act as natural nucleus for the melting process of the solid. "Surface melting" has indeed been observed for several unreconstructed fcc (110) surfaces; details are discussed in reference 68. The disordering sequence of enhanced anharmonicity, adatom-vacancy creation and thermal roughening appears to be the natural precur–sor to this phase transition.

In fig. 20 we show the results of a molecular dynamics simulation of the Cu(110) surface which nicely demonstrates the evolution from a well ordered flat surface through adatom-vacancy creation and roughening to surface melting upon approaching the bulk melting temperature [48]. In the snapshots of the equilibrium configuration of the Cu(110) surface adatoms begin to appear on the surface above 800 K (a) leading eventually to the onset of surface premelting with planar disorder at and above 1200 K (d,a). The snapshots between 1000 K and 1100 K (b,c) show the adatom clustering and the surface roughening.

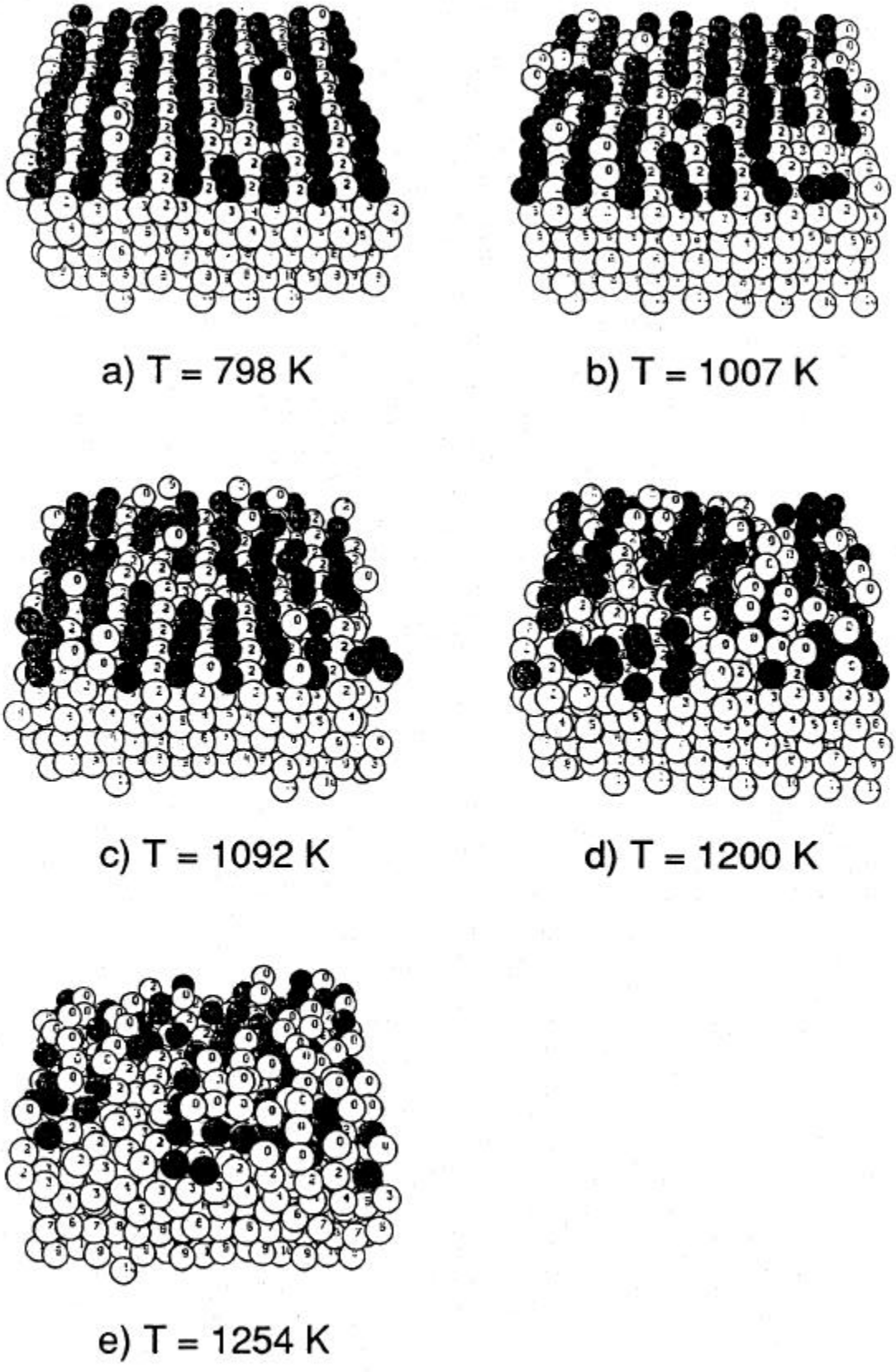

Figure 20. Molecular dynamics shapshots of configurations of the Cu (110) surface as a function of temperature [48]. The black atoms belong to the original surface layer.

4.2 Missing row-reconstructed fcc (110) (1 ×2) surfaces : Deconstruction versus roughening.

In the case of Au(110), the missing row (1×2) phase has been found to be stable only in a limited temperature range [69]. Upon heating, the half order superlattice LEED-spot was seen to change shape with temperature and eventually disappeared at a critical temperature $T_c \cong 0.49\ T_M \cong 650$ K, indicating a conti–nuous phase transition from an ordered (1×2) state into a disordered (1×1) phase. Campuzano et al. [69] have analyzed this phase transition in terms of a two dimen–sional order-disorder transition and determined critical exponents consistent with the predictions of the 2D-Ising model, which, due to the p2mm symmetry of the Au(110) (1×2) surface, is indeed the appropriate universality class [70].

A considerable amount of disorder, however has also been observed to be present in the low temperature missing row phase of all three metals Ir, Pt and Au [71,72]. While the coherence along the [1$\bar{1}$0] direction (parallel to the close packed rows) extends over several hundred Å, the coherence length along the [001] direction (perpendicular to the rows) hardly surpassed 100–200 Å. Scanning tunneling microscopy assigned this intrinsic disorder to the presence of some (1×3) and (1×4) reconstructed regions, which are induced by a micro (111) facetting.

In theoretical studies it has been shown that the (1×2) missing row configu–ration is indeed only marginally stable with respect to the "higher" missing row states (1×3, 1×4, ..., 1×n). The energy difference between any of the (1×n) phases of Au(110) has been calculated to be less than 10meV per atom [38]. Based on this ground it has been argued by several authors that the missing row configuration should be thermally unstable with respect to the formation of (111) microfacets, giving rise to a "rough" surface at elevated temperatures. While Villain and Vilfan [73] have predicted a succession of two transitions, an Ising-like order-disorder transition at ~ 0.50 T_M (spontaneous proliferation of antiphase Ising-defects, fig. 21) followed by roughening transition at ~ 0.57 T_M (onset of (111) micro facetting generating single height steps, fig. 21), Levi and Touzani [74] have found no evidence for an Ising-like transition but predicted a direct roughening transition.

In a recent x-ray diffraction experiment Robinson, Vlieg and Kern have studied the thermal behavior of the reconstructed Pt(110) surface [75,76]. The experimen–tally observed half order diffraction peaks have two characteristics : they are broad in the [001] direction but sharp in the orthogonal [1$\bar{1}$0] direction and always displaced slightly from the exact half order position along [001]. The uniaxial broadening and shift implies disorder in one direction only, i.e. must be associated with line defects oriented perpendicular to the [001] direction. An identical pattern of uniaxially shifted and broadened half order diffraction peaks was observed earlier by Robinson et al. [32] for the Au(110) surface and can be explained conclusively in terms of randomly distributed single height steps on the surface. It was further

demonstrated that the peak shift of the half order spots is directly related to the density of these monatomic steps [32,75], while Ising-like defects would only result in a symmetric peak broadening. Indeed, (111) micro facets are also the predominant defects seen in scanning tunneling microscopy images of Au(110) and Pt(110) [71,72].

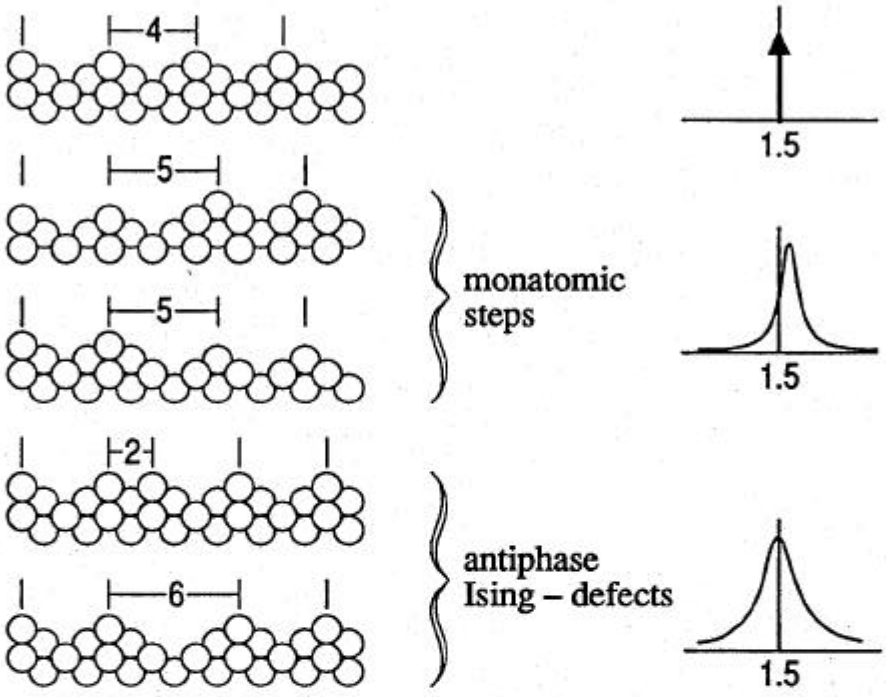

Figure 21. Thermal excitations of the fcc (110) (1 × 2) missing row reconstructed surface; Ising-like antiphase defects and monatomic steps, i.e. (111) microfacets. Also shown schematically is the profile of the half-order diffraction peak with and without defects.

The temperature dependence of the half-order diffraction profile was measured and found to behave reversibly. The data are summarized in fig. 22, clearly demonstrating a phase transition at a critical temperature of $T_c = 0.53 \quad T_M = 1080 \pm 1$ K. The peak height, I (T), is fully compatible with a theoretical curve $I(T) = I_o\, |t|^{2\beta'}$ where $t = T/T_c - 1$ and $\beta' = 0.11 \pm 0.01$. Above T_c the half-width diverges linearly with the reduced temperature. Both of these aspects are exactly in accord with the predictions of the 2D-Ising model, which has $\beta' = 1/8$ and $\nu = 1$ (correlation length exponent), and agree well with the LEED data for the analogous phase transition of Au(110) (1×2).

Notwithstanding this apparent agreement between Pt(110), Au(110) and the 2D Ising model, we now turn to the behavior of the diffraction peak shift in fig. 22. Above T_C the peak shifts substantially and completely reversibly.

Originally Robinson et al. interpreted this results to be in contrast to the Ising classification because it implies that an equilibrium density of steps appears spontaneously above T_c. This immediately implicates some roughening character. The slopes of the half-width and peak shift versus T in fig. 22 allow us to quantify the line defect density in units of probability per lattice site for the monatomic steps $\alpha = 6.6t$ and antiphase Ising defects $\beta = 2.8$ t; i.e. thermally induced steps are 2-3 times more common.

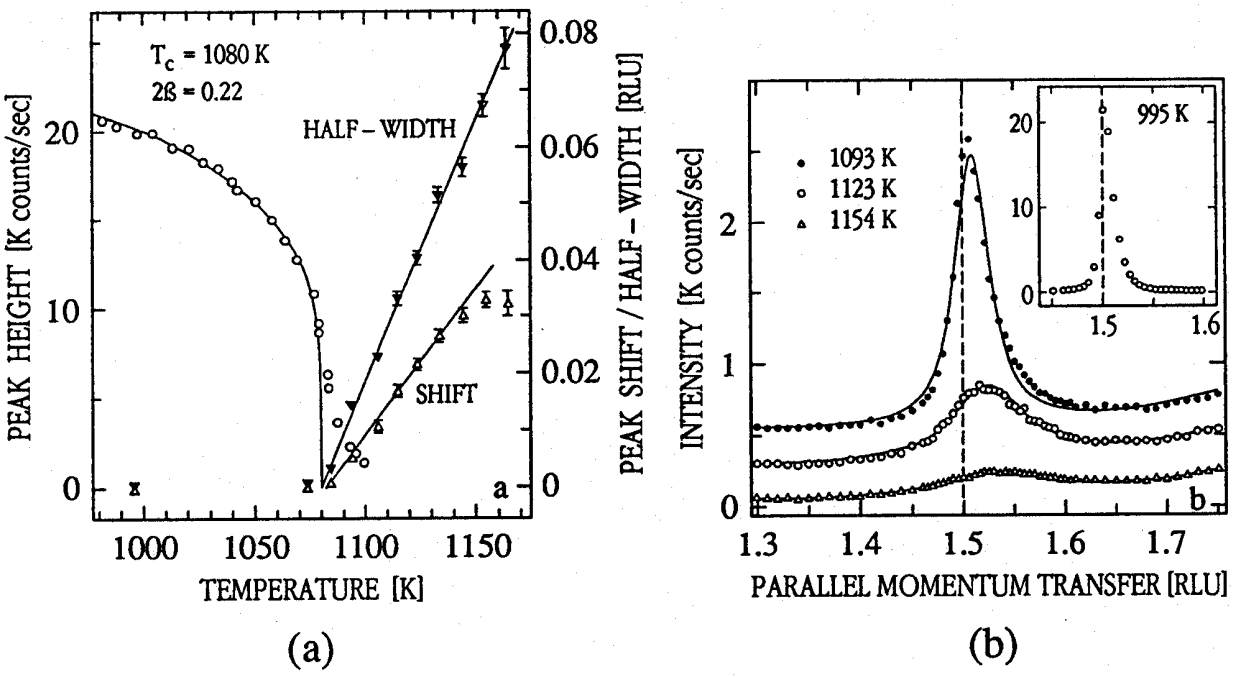

Figure 22. a) Temperature dependence of the half-order x-ray diffraction peak (h, 0.06, 0.06) from Pt (110) (1 × 2) obtained by scanning h [75]. b) Temperature dependence of the extracted peak height, width and shift [75].

Two solutions have been proposed to escape from this paradox. Villain and Vilfan [77] suggest that the steps formed above the transition are bound together in pairs. The imposition of paired steps leads necessarily to a phase transition model in the Ising-universality class due to the twofold degenerated ground state. This model forbids any height divergence and the surface is never rough. Villain and Vilfan suggest a step pair unbinding transition at higher temperatures $T_{c'} > T_c$ which eventually roughens the surface. Den Nijs [78], however, suggests a transition with real roughening character but Ising-criticality. In the framework of a 4-states chiral clock step model, den Nijs demonstrated that for negligible chirality the recons–tructed (1×2) (110) surface deconstructs and roughens in one single transition which is characterized by Ising exponents. This transition has the character of an incommensurate melting transition with respect to the reconstruction degrees of freedom, explaining the peak shift and the linear vanishing of it at T_c. Zero

chirality, however, requires that step defects with a phase shift of 3 half-cells (see fig. 21) have also to be present on the surface, but are rarely observed [71,72] and are expected to be energetically unfavorable [79].

More recently, Mazzeo et al. [80] demonstrated that a small diffraction peak shift in the initial phase of the transition might be obtained by a disordered flat phase with a random mixture of odd and even (1×n) configurations. In their simulation the Ising-disordering and the roughening are separated by about 30 K. At the roughening temperature they observe already a peakshift of 0.012 RLU. Assuming that the same shift would be characteristic for the roughening temperature of the Pt(110) surface, the x-ray measurements would support in fact the original Villain-Vilfan scenario of two separated transitions at $T_c = 1080$ K (Ising-disordering) and $T_R = 1110$ K (surface roughening).

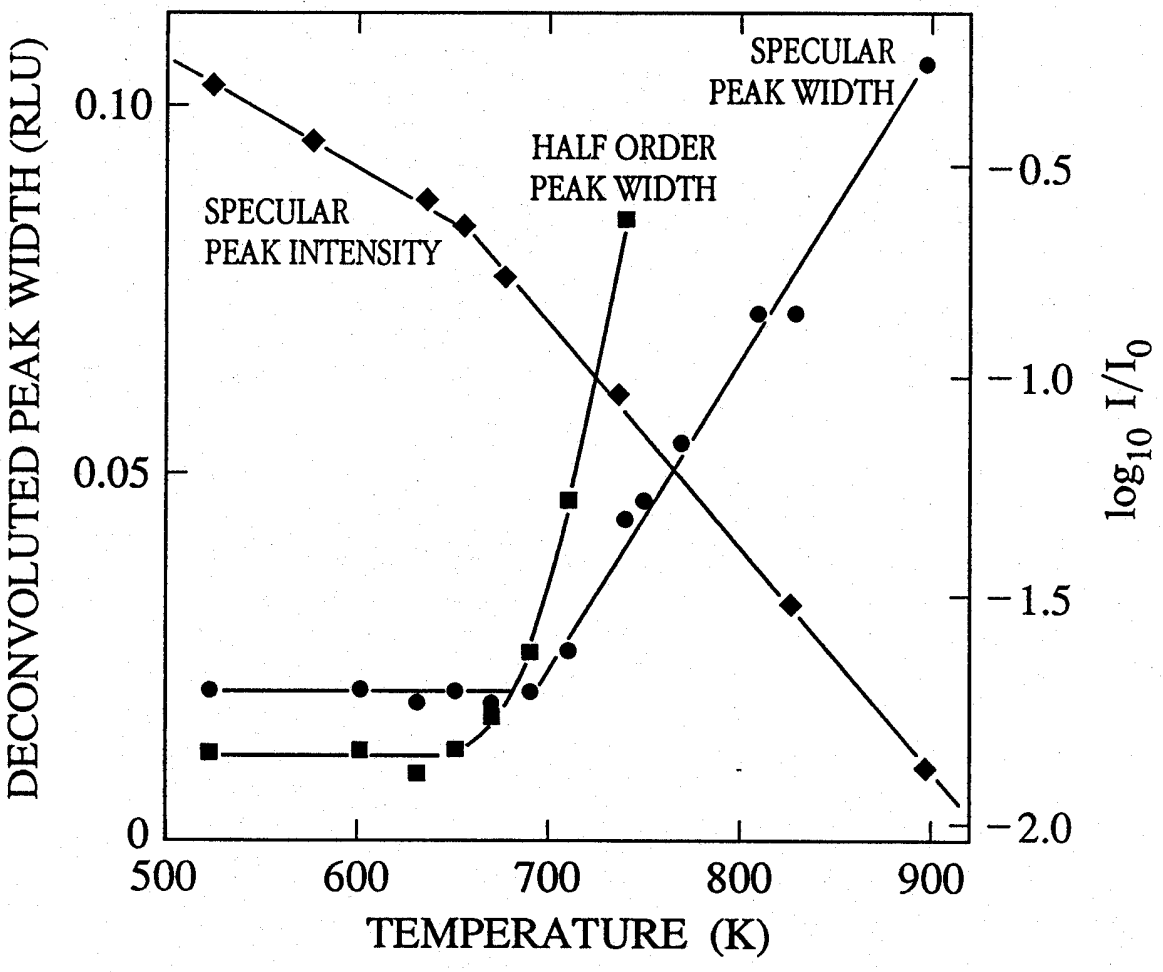

Figure 23. Intensity and peak-width of a He-beam diffracted from a Au (110) surface as a function of temperature [82] : diamonds - intensity of the specular in-phase peak, circles - width of the specular anti-phase peak and squares - width of the half-order diffraction peak under incidence conditions yielding minimum width.

Indeed, two recent He-diffraction studies of the Pt(110) (1×2) [81] and the Au(110) (1×2) [82] surface clearly support the model with two successive transi–tions. In the case of Pt(110) Krzyzowski et al. determine the transition temperature to be $T_c = 1030$ K and $T_R = 1090$ K, while for the Au surface Sprösser et al. find $T_c = 650$ K and $T_R = 650$ K. Both studies use the detailed analysis of the He peak-intensities, widths and line shapes measured for in-phase and anti-phase diffraction. As example we will discuss here the results for Au (110) (1×2) [82]. In fig. 23 we show the measured intensity and peak-width of the specular and the half-order He-diffraction peak. Between 100 K and 650 K both diffraction peak-widths and the specular intensity decrease exponentially (Debye-Waller behavior). At $T_c = 650$ K the half-order peak width increases rapidly and the specular intensity changes slope. The specular peak width, however, still remains constant up to 690 K and increases dramatically above $T_R = 690$ K. While the specular intensity and the half-order peak-width are sensitive to both in-plane Ising defects and steps, the specular peak-width (anti-phase) is sensing only steps. The observed thermal evolution clearly demonstrates the existence of two successive transitions. A detailed analysis of the experimental anti-phase specular profiles revealed power law line shapes above $T_R = 590$ K in agreement with eq. (8), indicating a logarithmic divergence of the height-height correlation function $g_\perp(r)$.

In summary, the experimental data for Au(110) (1×2) and Pt(110) (1×2) seem to support a two step-transition. First, the surface disorders laterally via the excitation of antiphase-Ising defects. The critical behavior of the transition is consistent with the 2D-Ising model. The surfaces roughen in a second transition distinct from the deconstruction to a state with logarithmic height-height correlation. The two phase transitions are separated by 40-50 K.

4.3 The close packed fcc (100) and (111) surfaces

The (111) and (100) faces of fcc-metals are the most densely packed surfaces. For a long time, it was believed that, in particular the close-packed (111) surfaces are ultimately stable and no structural changes were expected with increasing temperature. In recent experiments it was however demonstrated, that even the (111) surfaces have the tendency to reconstruct into compression structures caused by the energy gain due to the density increase of the outermost layer [83–85]. A driving mechanism of surface reconstruction which was already well established for (100) surfaces of transition metals (Au, Ir, Pt) [86]. While in the case of Au (111) the reconstruction occurs spontaneously [83] it is activated on the Pt (111) surface, where the reconstruction can be induced by a temperature increase [84] or through the enhancement of the Pt-gas phase chemical potential [85].

While the reconstruction behavior of the (100) and (111) fcc surfaces and its thermal dependence is an active field of research, studies of thermal roughening are very rare. Indeed, at least for the (111) surface energetic arguments strongly suggest that the roughening temperature should exceed the melting temperature of the material [9]. The only roughening study reported so far is the work of Abernathy et al. [87], who have investigated the Pt (100) surface at temperatures close to bulk melting. Their x-ray data, indeed, suggest a thermal roughening transition around $T_R \sim 0.9\ T_M$. Above 1800 K they observe diffraction peaks the profiles of which are consistent with the power-law lineshape of eq. (8), charac–terizing a rough phase with logarithmic diverging height-height correlations.

5 ROUGHENING OF VICINAL SURFACES

5.1 The kink free energy and step roughening

The microscopic mechanism which leads to the thermal roughening of a low (non vicinal) and a high Miller index (vicinal) surface is different [35, 88]. A low index surface fulfills the roughening condition, Eq. (1), when the free energy for the creation of a step β becomes zero. In contrast, on a vicinal surface - which at $T = 0$ K is already stepped – Eq. (1) can be fulfilled also without the creation of new steps. The elementary excitation of a vicinal surface is a bound pair of kinks in the step edge bordering a terrace. Such a pair of kinks is readily excited since its forma–tion costs only two broken bonds $2\ W_o$, while at close packed surfaces even the excitation of an adatom-vacancy pair costs four broken bonds. It is, indeed, the vanishing of W_o and the corresponding proliferation of kinks, which mark the roughening of vicinal surfaces.

It has been known for a long time that an isolated step is always unstable with respect to the formation of kinks for all temperatures $T \neq 0$ K, in other words, the roughening temperature T_R of isolated steps is always zero. However, in vicinal surfaces, i.e., surfaces with steps ordered into a superlattice of equally spaced monatomic steps, a second energy term, the step-step interaction energy ω_ℓ, enters. This step-step interaction has its origin in elastic as well as electrostatic forces. The surface lattice is distorted in the neighborhood of a step. At a closer distance the distortion fields of two approaching step interact and the steps repel each other. In addition, the local dipole-moment of a step differs from the terrace value, which likewise may result in forces between steps.

It is this repulsive interaction between two approaching steps which stabilizes the vicinal surfaces at low temperature.

This step-step interaction is repulsive on a short-range scale, but might become attractive at intermediate distances [65]. It is the repulsive interaction ω_ℓ between two neighboring steps which stabilizes the superlattice of equally

spaced steps at low temperature and which rises the roughening temperature to a nonzero value. At low temperatures, $T << T_R$, the surface has the regular array of straight steps shown in fig. 24. At higher temperatures thermal disorder through the generation of kinks competes with the order established by the repulsive step-step interaction. At the roughening temperature, kinks can be spontaneously proliferated and by adopting a large number of configurations (the steps meander) the surface increases its entropy and lowers its free energy. The creation of kinks on a vicinal surface leads to a broadening of the distribution of nearest neighbor step distances, while the repulsive step-step interaction tends to keep the nominal step-step distance on a local scale. The competition between these to effects leads to the formation of domains with the same structure as the perfect vicinal surface. The average level of a domain differs from that of the adjacent ones by an integer multiple of the unit vector; i.e. the lines of kinks from domain boundaries act as "secondary" steps (see fig. 25).

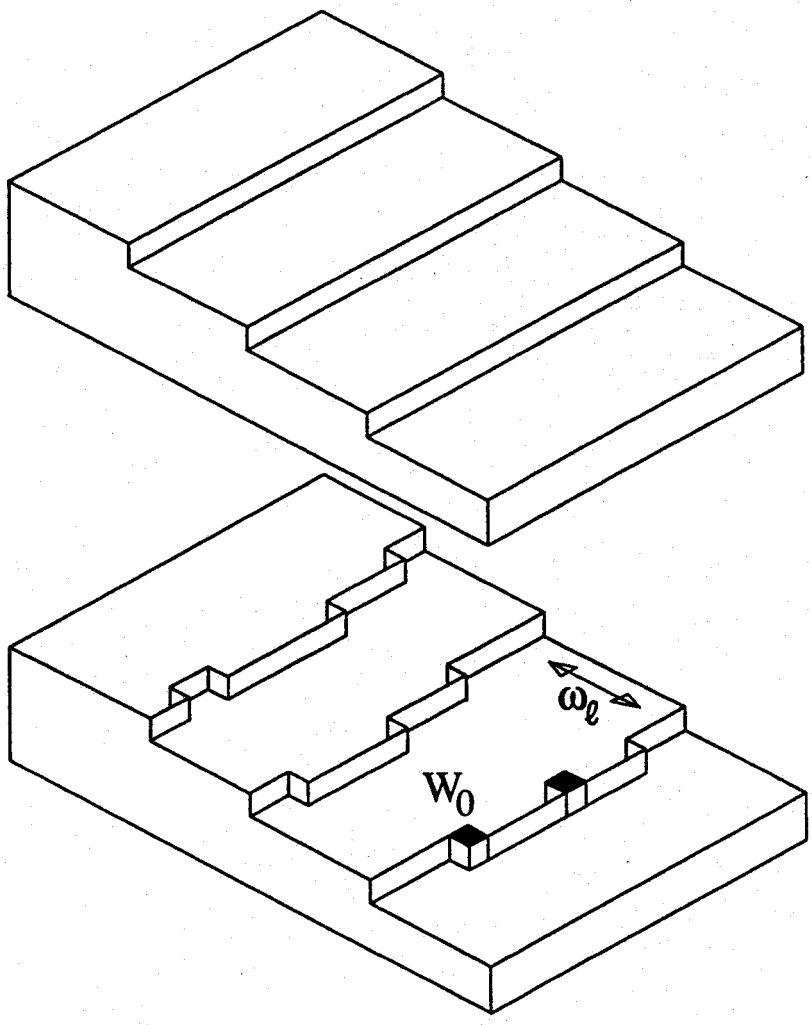

Figure 24. Topography of a vicinal surface at zero Kelvin (top) and above the roughening temperature (bottom).

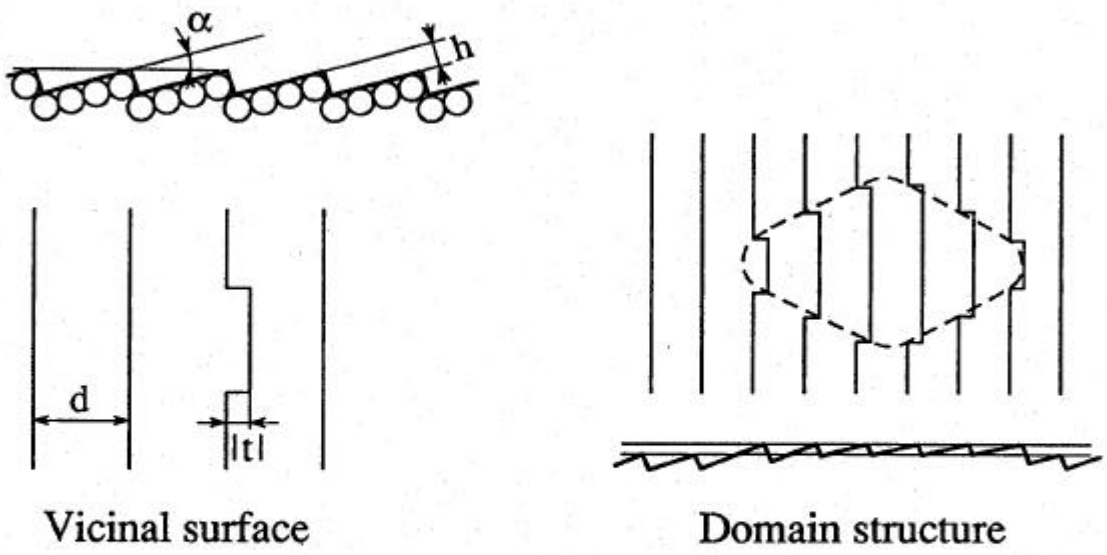

Figure 25. Elementary excitation of a vicinal surface (a) and domain organization of these elementary excitations (b).

The proliferation of "secondary" steps gives rise to the same logarithmic divergence of the height-height correlation function as observed for close packed surfaces and expressed by eq. (1). The roughening temperature is determined by the competition between the kink creation energy W_o and the step-step repulsion ω_ℓ. W_o is not expected to depend upon the step-step distance d. The step-step repulsion on the other hand depends strongly upon d since both elastic and electrostatic interactions scale inversely with the square of the distance. For the same family of vicinal surfaces the roughening temperature is thus expected to decrease when d increase.

5.2 The step roughening transition of fcc (11n) surfaces

Many stepped metal surfaces have been investigated during the last decade, most of them have fcc structure and belong to the (11n) type. This class of vicinal surfaces has densely packed (100) terraces separated by monoatomic steps running along [001] and spaced regularly with a periodicity $d = n\,a/2$ (with $n = 3, 5, 7, \ldots$).

The first piece of evidence that a roughening transition might occur on these vicinal metal surfaces was reported in 1982 by Lapujoulade et al. [89]. They observed a dramatic drop in the He-intensity coherently scattered from the Cu (115) surface upon increasing the temperature above ~ 400 K. This behavior contrasted with the generally observed, much weaker decrease of the coherent intensity, accounted for by the Debye-Waller factor [30]. Lapujoulade and co–workers claimed that this anomalous behavior was due to thermal roughening and assigned the temperature at which the data deviate from the Debye-Waller behavior to the roughening temperature. As

was demonstrated in chapter 4.1.1 such anomalous behavior, however, can have other causes, but for Cu (115) this assignment happened to be correct.

More sound experimental arguments for the existence of a roughening transition of vicinal metal surfaces were reported a few years later in a series of detailed He- and x-ray-diffraction studies [90-99]. In fig. 26 we show the result of a x-ray diffraction study of Liang et al. [94] who investigated the Cu (113) surface. The data show the measured integrated intensity of the x-ray diffraction peak under anti-phase scattering conditions. The temperature at which the diffracted intensity disappears was identified with the roughening transition yielding a roughening temperature $T_R = 620 \pm 10\ K = 0.46\ T_M$.

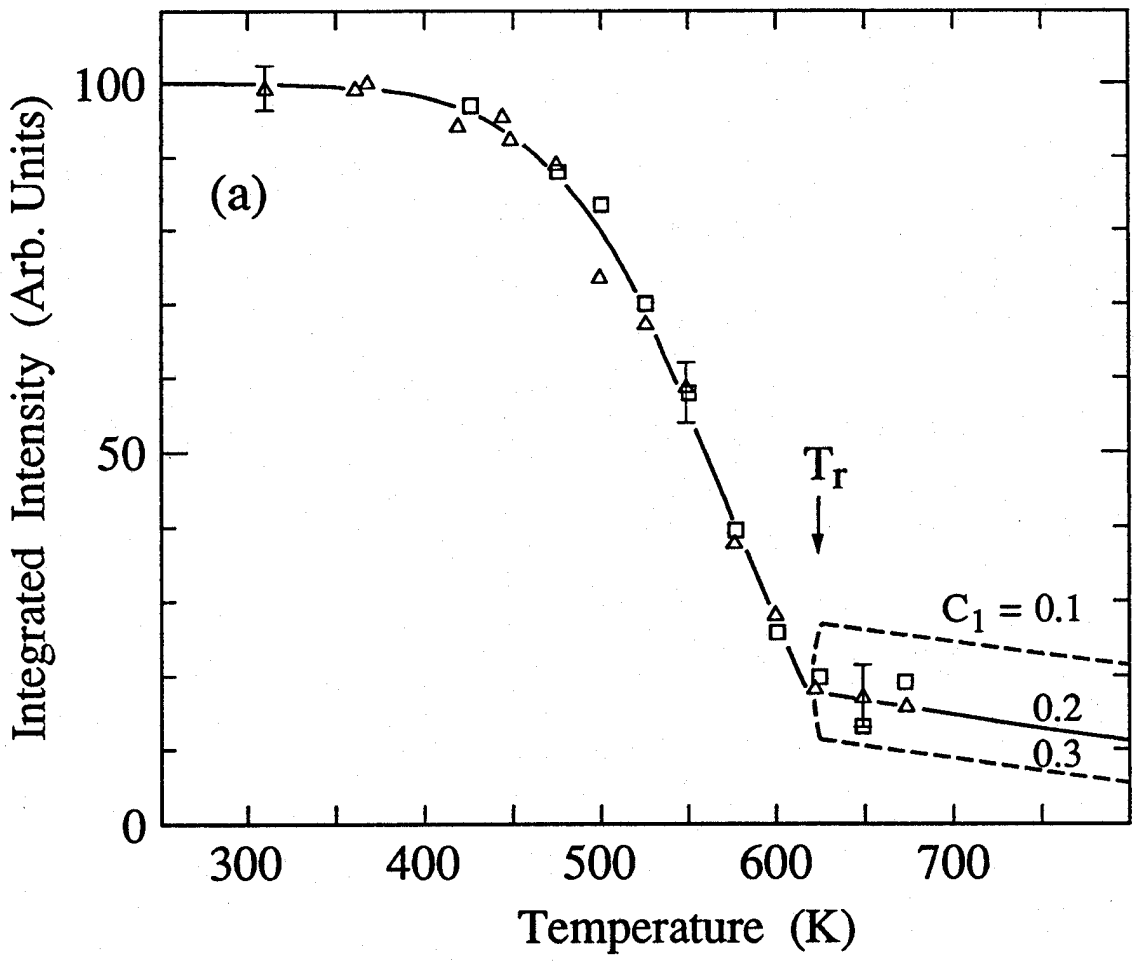

Figure 26. Integrated intensity of the x-ray "step-superlattice" diffraction from the Cu (113) surface [94].

The same surface was also investigated by He-diffraction [90]. The width of the specular peak in anti-phase geometry was found to oscillate with the incidence angle, showing that the thermally generated disorder on Cu (113) is due to the excitation of kinks. Peak profiles were measured and their shape was found in good agreement (in the thermally rough phase) with the

prediction of eq. (8). In fig. 27 we show the deduced roughening exponent versus temperature indicative of a roughening temperature of $T_R = 720 \pm 50$ K.

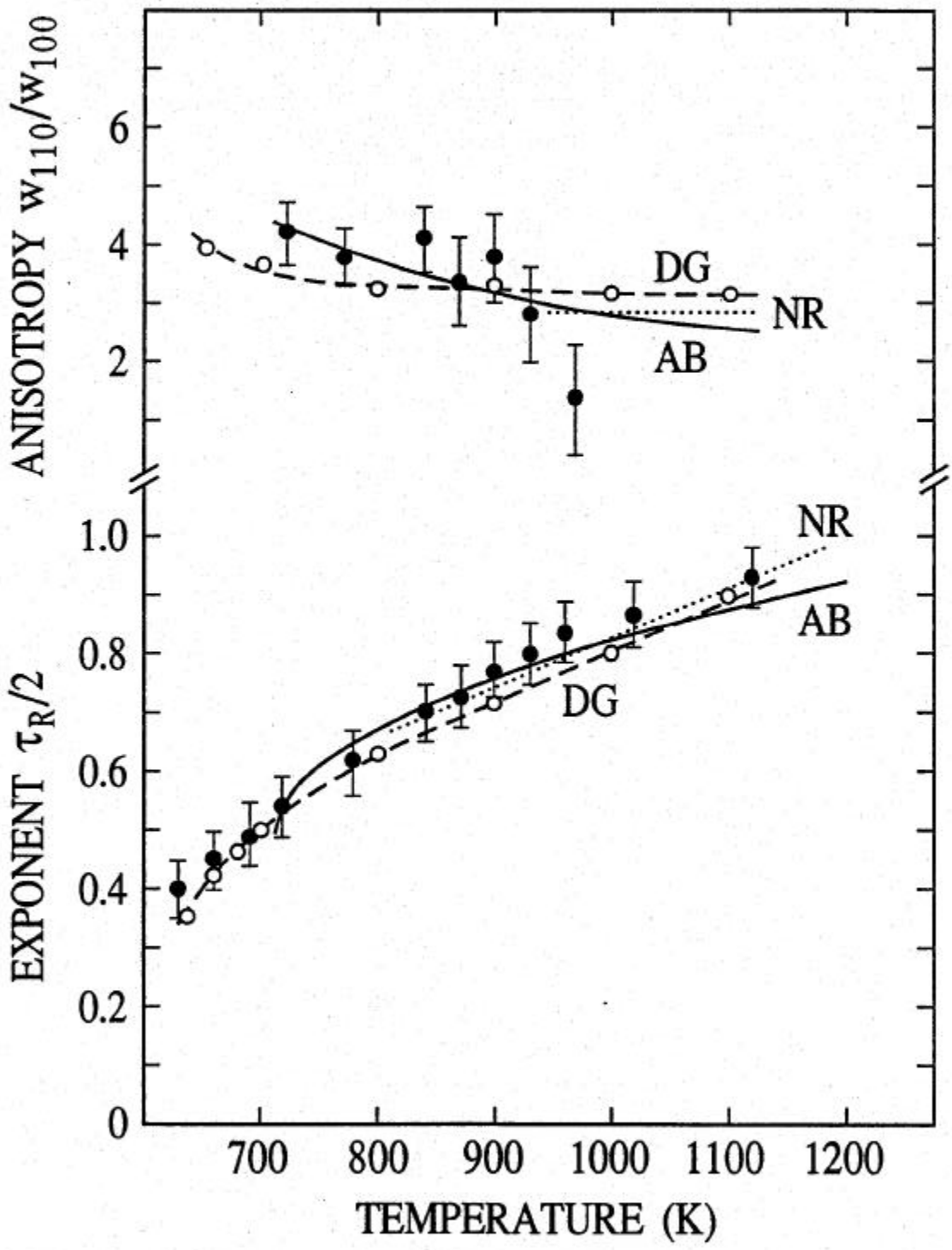

Figure 27. Roughening exponent $\tau_R/2$ and diffraction peak anisotropy w_{110}/w_{100} of Cu (113) deduced from a detailed analysis of measured He-diffraction line shape [90].

Salanon et al. [90] also measured in their study a significant diffraction peak anisotropy (see upper part of fig. 27). The diffracted He-peaks are found to be much broader in the [110] direction than in the [001] direction., Intuitively one expects from the geometrical anisotropy of the vicinal (11n) surfaces (the lattice constant along the step a is much smaller than the distance between neighboring steps d) the inverse behavior, i.e. an enhanced broadening in the direction parallel to the steps. The experimental results thus indicate, that the geometrical anisotropy is overcompensated by the energetic anisotropy acting in the opposite sense. This energetic anisotropy reflects the energy difference between the step rigidity against kink creation and the step-step interaction. The observed enhanced peak broadening along [110] indicates thus, that the step rigidity ω_{sr}, which is related to the kink formation energy through $\omega_{sr} = 1/2\ k_B T \exp(W_o/k_B T)$, is larger than the step-step repulsion ω_ℓ. A quantitative analysis revealed a kink formation energy of $W_o = 800 \pm 50$ K and a repulsive step-step interaction energy of $\omega_\ell = 560 \pm 50$ K. This energetic anisotropy of $W_o/\omega_\ell \approx 1.4$ is, however, not consistent with the much larger anisotropy of $W_o/\omega_\ell \approx 32$ deduced for the same surface in the x-ray diffraction study of Liang et al. [94]. Indeed, also the observed roughening temperatures are off by 100 K. This difference might be related to experimental ambiguities in the He-diffraction experiments. The He-data being obtained with an energy integrating detector, Salanon et al. did not account for inelastic effects. One-phonon and multiphonon scattering, which are certainly important He-scattering contributions at elevated temperatures close to T_R, might substantially contribute to the measured line-shapes.

The agreement between x-ray and He-diffraction data is indeed much closer in the case of Ni (113). Here, the analysis of the He-diffraction lineshape had been corrected for inelastic contributions. The estimated roughening temperatures of 750 ± 50 K (He-diffraction [95]) and 740 K (x-ray diffraction [97]) agree nicely. In table II we have summarized the observed roughening transitions of vicinal metal surfaces. As far as a quantitative analysis of the energetic parameters has been done, the values of the kink creation energy and the step-step interaction has been included.

The roughening of the Ag (115) surface was deduced from a scanning tunneling microscopy study imaging directly the topography of the step edges [98]. The results of Frenken et al. are shown in fig. 28. In the STM-images at 293 K and 331 K large (115) terraces are observed with a low density of misorientation steps. In the images above 271 K all steps have a large number of thermally generated kinks and the observed step meandering indicates that the Ag (115) surface is already thermally roughened.

Table 2
Roughening temperatures of vicinal metal surfaces

Surface	T_R [K]	W_0 [K]	ω_ℓ [K]	technique	reference
Cu (113)	720	800	560	He	90
	620	2100	65	x-ray	94
Cu (115)	380	850	120	He	91
Cu (1111)	< 300		~ 5	He	92
			~ 1	STM	106
Ni (113)	750			He	95
	740	3500	55	x-ray	97
Ni (115)	450			He	96
Ag (115)	350			STM	98
Cu (331)	650	~1000	~ 500	He	93
Cu (310)	< 300	~ 400	~ 300	He	93
Pt (997)	~ 1050			STM	99

The results presented above for the family of the fcc (11n) surfaces are all in agreement with the terrace-step-kink (TSK) roughening model of vicinal surfaces. Recent experiments of Lapujoulade's group for the (331) and (310) surfaces of copper also fall in this line and can be modeled with the TSK-theory [93].

A recent investigation of the vicinal Pt (997) surface is however not consistent with TSK-roughening via the formation of "secondary" steps. In their STM-study Hahn et al. [99] observed a roughening transition at $T_R \sim 950$ K. The thermally generated roughness on Pt (997) is however of different nature : the roughening proceeds via the spontaneous formation of hillocks with close packed [111] and [11$\bar{1}$] facets.

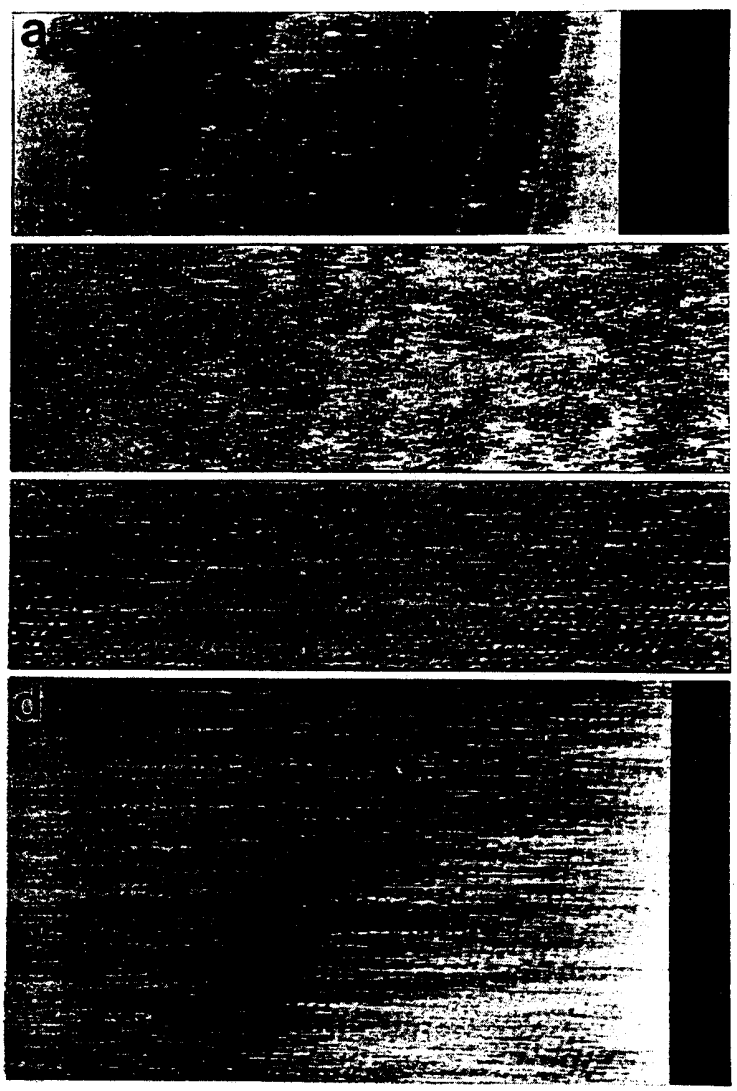

Figure 28. Scanning tunneling microscopy images of the Ag (115) surface as a function of temperature. a) 293 K, 585×220 Å^2, b) 331 K, 1180×375 Å^2, c) 371 K, 450×120 Å^2 and d) 418 K, 465×280 Å^2 [98].

6 CONSEQUENCES OF SURFACE ROUGHENING ON CRYSTAL GROWTH

6.1 Thin film epitaxy

Predicting the morphology and structure of a thin film epitaxially grown on a single-crystal surface has been a continuing challenge. The major goal is to understand the microscopic details of the growth processes to improve the properties of the epitaxial films. It is generally accepted that there are three types of growth possible [100]. In the Volmer-Weber (VW) growth, three dimensional islands grow. In the Frank-van der Merwe (FM) growth the film grows in a layer-by-layer fashion and in the Stranski-Krastanov (SK) growth 3D islands nucleate on top of a few epitaxially grown layers.

The FM-growth is clearly the preferred mode in thin-film epitaxy. In a simple thermodynamic model the FM-growth mode is expected for adlayers with low surface free energy relative to the substrate [101]. In an equilibrium experiment we would observe a series of first order phase transition in the pressure-temperature phase space, each associated with the adsorption of the n-th layer. As a function of temperature the vapor-pressure of the material to be grown will reveal a series of steps, each plateau of p_n (T) being the characteristic vapor pressure of the n-th adsorbate layer. At $p = p_n$ (T) the amount of adsorbed material jumps discontinuously from the value of the (n–1)-th layer to that of the n-th layer (see fig. 29). For each layer there exists, however, a critical temperature T_n^c above which the growth of the n-th layer does not proceed through a nucleation mechanism but through continuous growth [102]. In the limit of an infinite number of layers $n \rightarrow \infty$, the critical layer temperatures converge to the roughening temperature of the corresponding surface of a pure adsorbate crystal; i.e. $T^c_{n\rightarrow\infty} = T_R$. This convergence to the roughening temperature is directly related to the vanishing of the nucleation barrier above T_R [7]. From the practical point of view, epitaxially films can thus grow only in a FM-mode if the deposition temperature is below the roughening temperature of the growing surface.

The influence of the thermal roughening on thin film epitaxy was demonstrated in an elegant experiment of Miranda et al. [103] investigating the growth of Xe-multilayers on a stepped Pd surface. They used the layer-distinctive Xe 5p photoemission signal to measure Xe-adsorption isotherms as well as the relative equilibrium population of individual Xe-layers. At a temperature of 68 K they observed a distinct transition from layer-by-layer to continuous growth, identifying this temperature with the roughening temperature of the Xe-film surface.

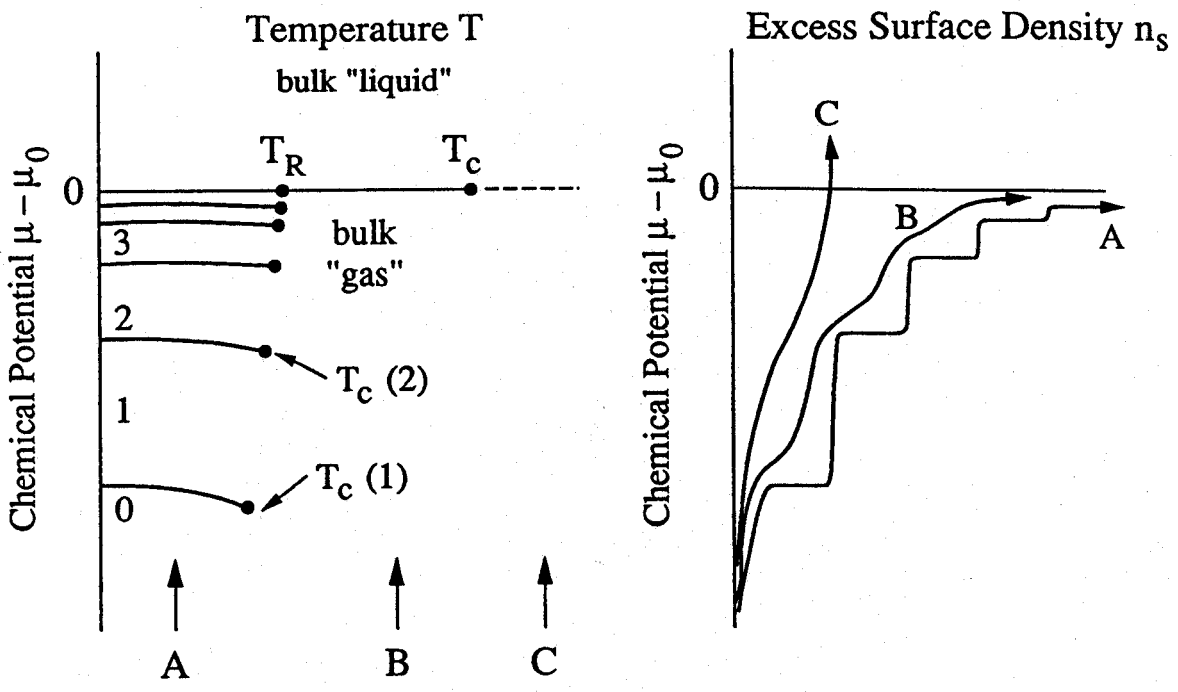

Figure 29. Schematic wetting phase-diagram for adlayers with low surface free energy relative to the substrate [102].

6.2 *Crystal growth and ECS*

As the roughening transition has consequences in thin film epitaxy it has consequences for crystal growth, in particular with respect to the resulting equilibrium crystal shape (see also chapter 2) [16, 104]. The growth of a smooth and a rough ($T > T_R$) surface is indeed very different. A rough surface is disordered, it has a significant density of adatom-vacancy pairs and kinked steps and the growth may proceed by the sticking of impinging atoms on the many defect sites present. This gives rise to a fast and linear growth [7]. The growth rate of a smooth surface below its roughening temperature, which is controlled by two-dimensional nucleation, is much smaller. Hence, as growth proceeds, the slowest growth faces are developed at the expense of the fast ones (rough and rounded). The final growth shape is, thus, made out of flat facets only. Because fewer and fewer facets are rough at lower temperature the growth shape is temperature dependent. The lower the temperature, the richer is the ECS. This is illustrated in fig. 30 showing the growth shapes of In-crystals as a function of temperature [105].

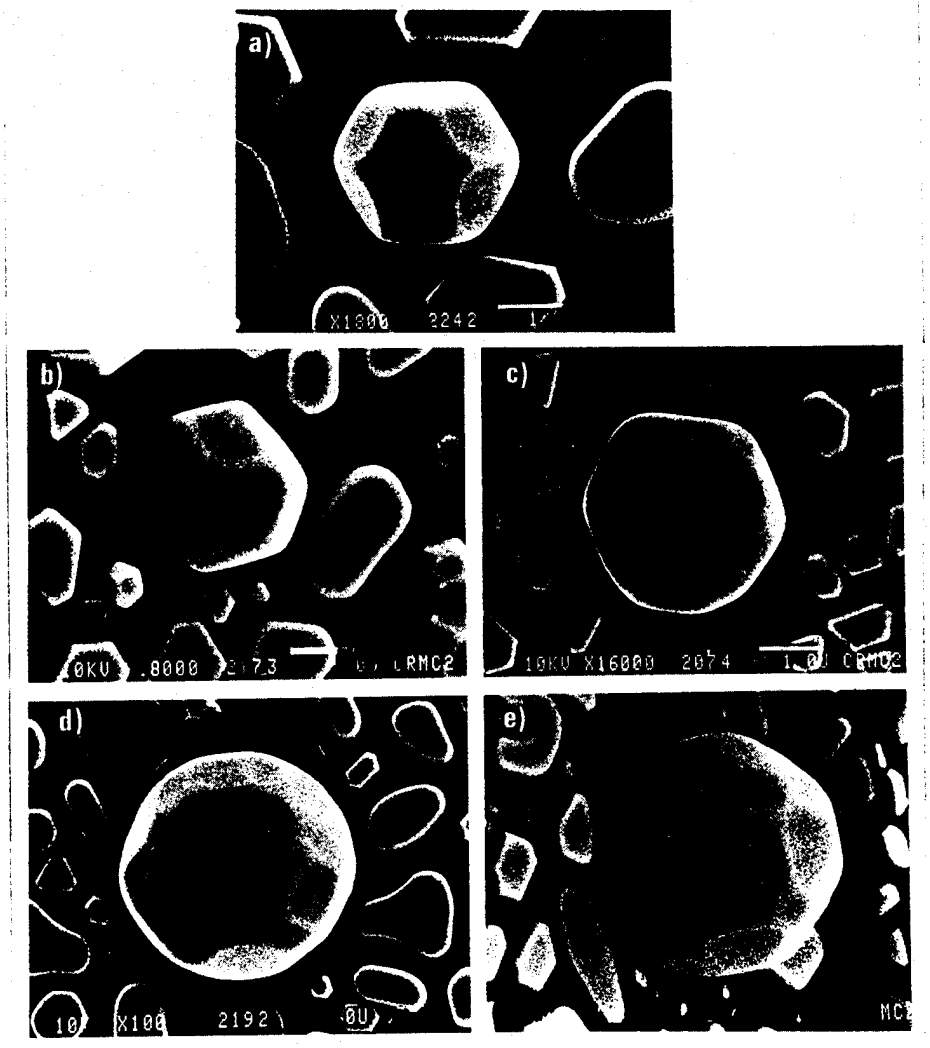

Figure 30. Growth shape of In crystals as a function of temperature [105], a) > 373 K, b) 313 K – 373 K, c) 293 K – 313 K, d) 283 K – 293 K, and e) < 283 K.

References

1 M.W. Finnis and V.J. Heine, J. Phys. F 4 (1974) L37.
2 J.E. Inglesfield, Prog. Surf. Sci. 20 (1985) 105.
3 J.F. van der Veen, B. Pluis and A.W. Denier van der Gon, in: Physics and Chemistry at Solid Surfaces VII, Springer, Berlin, 1988, p. 455.
4 F.A. Lindemann, Z. Phys. 14 (1910) 609.
5 J. Frenkel, J. Phys. USSR 9 (1945) 392.
6 W.K. Burton, N. Cabrera, Disc. Faraday Soc. 5 (1949) 33.
7 W.K. Burton, N. Cabrera and F.C. Frank, Philos. Trans. Roy. Soc. London 243 A (1951) 299.
8 R.W. Swendson, Phys. Rev. B 17 (1978) 3710.
9 H. van Beijeren and I. Nolden, in; Structure and Dynamics of Surfaces II, Springer, Berlin, 1986, p. 259; and references therein.
10 S. Balibar and B. Castaing, Surf. Sci. Rep. 5 (1985) 87.
11 F. Fabre, D. Gorse, B. Salanon and J. Lapujoulade, J. Physique 48 (1987) 1017.
12 E.H. Conrad, L.R. Allen, D.L. Blanchard and T. Engel, Surf. Sci. 187 (1987) 265.
13 G. Wulff, Z. Kristallogr. Mineral 34 (1901) 449.
14 C. Herring, Phys. Rev. 82 (1951) 87.
15 J.C. Heyraud and J.J. Métois, Surf. Sci. 128 (19??) 334.
16 M. Wortis, in: R. Vanselow and R. Howe (Eds.), Chemistry and Physics of Solid Surfaces VII, Springer, Berlin, 1988, p. 367.
17 F. Gallet, P. Nozières, S. Balibar and E. Rolley, Europhys. Lett. 2 (1986) 701.
18 J. Landau, S.G. Lipson, L.M. Maattanen, L.S. Balfour and D.O. Edwards, Phys. Rev. Lett. 45 (1980) 31.
S. Balibar and B. Castaing, J. Phys. Lett. 41 (1980) L329.
19 C. Rottman, M. Wortis, J.C. Heyraud and J.J. Métois, Phys. Rev. Lett. 52 (1984) 1009.
20 J.J. Saenz and N. Garcia, Surf. Sci. 155 (1985) 24.
21 J.C. Heyraud, J.J. Métois and J.M. Bernard, J. Cryst. Growth 98 (1989) 355.; J. Microsc. Spectrosc. Electron. 14 (1989) 343.
22 T.T. Tsong, Prog. Surf. Sci. 10 (1980) 165.
23 E. Bauer, Ultramicroscopy 17 (1985) 51.
W. Telieps and E. Bauer, Ultramicroscopy 17 (1985) 57.
24 G. Binnig and H. Rohrer, Physica 127 B (1984) 37.
H.J. Güntherhodt and R. Wiesendanger, (Eds), Scanning Tunneling Microscopy I & II, Springer, Berlin, 1992.
25 H. Roeder, E. Hahn and K. Kern, unpublished.
26 M.A. Van Hove, W.H. Weinberg and C.M. Chan, Low-Energy-Electron Diffraction, Springer, Berlin, 1986.
27 I.K. Robinson and D.J. Tweet, Rep. Prog. Phys. 55 (1992) 599.
28 E. Hulpke (Ed.), Helium Atom Scattering from Surfaces, Springer, Berlin, 1992.
29 M. Henzler, Appl. Surf. Sci. 11/12 (1982) 450.
30 B. Poelsema and G. Comsa, Scattering of Thermal Energy Atoms from Disordered Surfaces, Springer, Berlin, 1989.

31 M.G. Lagally, in: Methods of Experimental Physics, vol. 22, Academic, New York, 1985, p. 237.

32 P. Fenter and T.M. Lu, Surf. Sci. 154 (1985) 15.
I.K. Robinson, Y. Kuk and L.C. Feldman, Phys. Rev. B 29 (1984) 4762.

33 B. Poelsema, R.L. Palmer, G. Mechtersheimer and G. Comsa, Surf. Sci. 117 (1982) 50.

34 H.N. Yang, T.M. Lu and G.C. Wang, Phys. Rev. Lett. 63 (1989) 1621.

35 J.D. Weeks, in: T. Riste (Ed.), Ordering in Strongly Fluctuating Condensed Matter Systems, Plenum, New York, 1980, p. 293.
J. Villain, D.R. Grempel and J. Lapujoulade, J. Phys. F 15 (1985) 809.

36 P. Fery, W. Moritz and D. Wolf, Phys. Rev. B 38 (1988) 7275.

37 A. Trayanov, A.C. Levi and E. Tosatti, Europhys. Lett. 8 (1989) 657.
M. den Nijs, Phys. Rev. Lett. 64 (1990) 435.

38 M. Garofalo, E. Tosatti and F. Ercolessi, Surf. Sci. 188 (1987) 321.

39 R.S. Williams, P.S. Wehner, J. Stöhr and D.A. Shirley, Phys. Rev. Lett. 39 (1977) 302.

40 Th. Fauster, R. Schneider, H. Dürr, G. Engelmann and E. Taglauer, Surf. Sci. 189/190 (1987) 610.

41 S.G.J. Mochrie, Phys. Rev. Lett. 62 (1987) 63.

42 P. Zeppenfeld, K. Kern, R. David and G. Comsa, Phys. Rev. Lett. 62 (1989) 63.

43 J. Lapujoulade, J. Perreau and A. Kara, Surf. Sci. 129 (1983) 59.

44 K. Kern, U. Becher, J. George, P. Zeppenfeld and G. Comsa, to be published.

45 L. Yang and T.S. Rahman, Phys. Rev. Lett. 67 (1991) 2327.

46 E.T. Chen, R.N. Barnett and U. Landmann, Phys. Rev. B 41 (1990) 439.
P. Stoltze, J. Norskov and U. Landmann, Surf. Sci. 220 (1989) L693.

47 J.W.M. Frenken, F. Huussen and J.F. van der Veen, Phys. Rev. Lett. 58 (1985) 401.

48 H. Häkkinen and M. Manninen, Phys. Rev. B, in press.

49 H. Dürr, R. Schneider and Th. Fauster, Phys. Rev. B 43 (1991) 12187.

50 Y. Cao and E.H. Conrad, Phys. Rev. Lett. 64 (1990) 447.

51 M. den Nijs, Phys. Rev. Lett. 64 (1990) 435.

52 H.P. Bonzel, U. Breuer and M. Wortis, Surf. Sci. 259 (1991) 314.

53 A. Trayanov, A.C. Levi and E. Tosatti, Surf. Sci. 233 (1990) 184.

54 T. Michely, T. Land, U. Littmark and G. Comsa, Surf. Sci. 272 (1992) 204.

55 K. Kern, in: H. Taub et al. (Eds.), Phase Transitions in Surface Films 2, Plenum, New York, 1991, p. 265.

56 H.P. Bonzel and E. Latta, Surf. Sci. 76 (1978) 275.

57 H.P. Bonzel, in: Vu Thien Binh (Ed.), Surface Mobilities on Solid Materials, Plenum, New York, 1988, p. 195.

58 H.P. Bonzell, N. Freyer and E. Preuss, Phys. Rev. Lett. 57 (19??) 1024.

59 J.C. Heyraud and J.J. Métois, J. Cryst. Growth 82 (1987) 269.

60 G.A. Held, J.L. Jordan-Sweet, P.M. Horn, A. Mak and R.J. Birgeneau, Phys. Rev. Lett. 59 (1987) 2075.

61 S.M. Francis, N.V. Richardson, Phys. Rev. B 33 (1986) 662.

62 A.M. Lahee, J.P. Toennies, Ch, Wöll, Surf. Sci. 191 (1987) 529.
K.H. Rieder, private communication.

63 I.K. Robinson, E. Vlieg, H. Hornis and E.H. Conrad, Phys. Rev. Lett. 67 (1991) 1890.

64 J.F. Wolf, B. Vicenzi and H. Ibach, Surf. Sci. 249 (1991) 233.

65 J. Frohn, M. Giessen, M. Poensgen, J.F. Wolf and H. Ibach, Phys. Rev. Lett. 67 (1991) 3543.
66 J.F. Wolf, doctoral thesis, Aachen (1990).
67 A. Pavlovska and E. Bauer, Appl. Phys. A 51 (1990) 172.
68 J.F. Van der Veen, in: Phase Transitions in Surface Films 2, Plenum, New York, 1991, p. 289.
69 J.C. Campuzano, M.S. Foster, G. Jennings, R.F. Willis and W. Unertl, Phys. Rev. Lett. 54 (1985) 2684.
70 P. Bak, Solid State Commun. 32 (1979) 581.
71 G. Binnig, H. Rohrer, Ch. Gerber and E. Weibel, Surf. Sci. 131 (1983) L379.
72 T. Gritsch, D. Coulman, R.J. Behm and G. Ertl, Surf. Sci. 257 (1991) 297.
73 J. Villain and I. Vilfan, Surf. Sci. 199 (1988) 165.
74 A.V. Levi and M. Touzani, Surf. Sci. 218 (1989) 223.
75 I.K. Robinson, E. Vlieg and K. Kern, Phys. Rev. Lett. 63 (1989) 2578.
76 K. Kern, I.K. Robinson and E. Vlieg, Vacuum 41 (1990) 318.
77 J. Villain and I. Vilfan, Phys. Rev. Lett. 65 (1990) 1830.
78 M. den Nijs, in: H. Taub et al. (Eds), Phase Transitions in Surface Films 2, Plenum, New York, 1991, p. 247.
79 L.D. Roelofs, S.M. Foiles, M.S. Daw and M. Baskes, Surf. Sci. 234 (1990) 63.
80 G. Mazzeo, G. Jug, A.C. Levi and E. Tosatti, Surf. Sci. 273 (1992) 237.
81 M. Krzyzowski, K. Kern, P. Zeppenfeld, Ch. Romainczyk and G. Comsa, to be published.
82 J. Sprösser, B. Salanon and J. Lapujoulade, Europhys. Lett. 16 (1991) 283.
83 J.V. Barth, H. Brune, G. Ertl and R.J. Behm, Phys. Rev. B 43 (1990) 9307.
84 A.R. Sandy, S.G.J. Mochrie, D.M. Zehner, G. Grübel, K.G. Huang and D. Gibbs, Phys. Rev. Lett. 68 (1992) 2192.
85 M. Bott, M. Hohage, T. Michely and G. Comsa, to be published.
86 M.A. Van Hove, R.J. Koestner, P.C. Stair, J.P. Biberain, L.L. Kesmodel, I. Bartos and G.A. Somorjai, Surf. Sci. 103 (1981) 189.
87 D.L. Abernathy, S.G.J. Mochrie, D.M. Zehner, G. Grubel and D. Gibbs, Phys. Rev. B 45 (1992) 9272.
88 W. Selke and A.M. Szpilka, Z. Phys. B 62 (1986) 381.
89 J. Lapujoulade, J. Perreau and A. Kara, Surf. Sci. 129 (1983) 59.
90 B. Salanon, F. Fabre, J. Lapujoulade and W. Selke, Phys. Rev. B 38 (1988) 7385.
91 F. Fabre, D. Gorse, J. Lapujoulade and B. Salanon, Europhys. Lett. 3 (1987) 737; J. Physique (Paris) 48 (1987) 1017.
92 F. Fabre, B. Salanon and J. Lapujoulade, Solid State Commun. 64 (1987) 1125.
93 B. Loisel, thesis, Paris (1989).
94 K.S. Liang, E.B. Sirota, K.L. D'Amico, G.J. Hughes and S.K. Sinha, Phys. Rev. Lett. 59 (1987) 2447.
95 E.H. Conrad, L.R. Allen, D.L. Blanchard and T. Engel, Surf. Sci. 187 (1987) 265.
96 E.H. Conrad, R.M. Aten, D.S. Kaufman, L.R. Allen, T. Engel, M. den Nijs and E.K. Riedel, J. Chem. Phys. 84 (1986) 1015, Erratum 85 (1986) 4856.
97 I.K. Robinson, E.H. Conrad and D.S. Reed, J. Physique (Paris) 51 (1990) 103.
98 J.W.M. Frenken, R.J. Hamers and J.E. Demuth, J. Vac. Sci. Technol. A8 (1990) 293.

99 E. Hahn, A. Fricke, H. Röder and K. Kern, to be published.
100 J.A. Venables, G.D.T. Spiller and M. Hanbücken, Rep. Prog. Phys. 47 (1984) 399.
101 E. Bauer, Appl. Surf. Sci. 11/12 (1982) 479.
102 R. Pandit, M. Schick and M. Wartis, Phys. Rev. B 26 (1982) 5112.
103 R. Miranda, E.V. Albano, S. Daiser, K. Wandelt and G. Ertl, Phys. Rev. Lett. 51 (1983) 782; J. Chem. Phys. 80 (1984) 2931.
104 M. Bienfait, Surf. Sci. 272 (1992) 1.
105 J.C. Heyraud and J.J. Métois, J. Cryst. Growth 82 (1987) 269.
106 S. Rousset, S. Gauthier, O. Siboulet, J.C. Girard, S. de Cheveigné, M. Huerta-Garnica, W. Sacks, M. Belin and J. Klein, Ultramicroscopy 42-44 (1992) 515.